Air Quality Impacts of the 2018 Mt. Kilauea Volcano Eruption in Hawaii: A Regional Chemical Transport Model Study with Satellite-Constrained Emissions

Youhua Tang[1,2], Daniel Q. Tong[1,2,3], Kai Yang[4], Pius Lee[1], Barry Baker[1,2], Alice Crawford[1], Winston Luke[1], Ariel Stein[1], Patrick C. Campbell[1,2], Allison Ring[1,4], James Flynn[4], Yuxuan Wang[5], Jeff McQueen[6], Li Pan[6,7], Jianping Huang[6,7] and Ivanka Stajner[6]

1. NOAA Air Resources Laboratory, 5830 University Research Court, College Park, MD.
2. Center for Spatial Information Science and Systems, George Mason University, Fairfax, VA.
3. Department of Atmospheric, Oceanic and Earth Sciences, George Mason University, Fairfax, VA.
4. University of Maryland, College Park, MD.
5. Dept. of Earth and Atmospheric Sciences, University of Houston, Houston, TX
6. NOAA National Centers for Environmental Prediction (NCEP), College Park, MD
7. I.M. Systems Group Inc., Rockville, MD

Corresponding authors: Youhua Tang (Youhua.Tang@noaa.gov); Daniel Q. Tong (qtong@gmu.edu)

Abstract

Volcanic eruptions could bring a vast amount of sulfur dioxide (SO_2) and ash into the air, often imposing substantial impacts on air quality and the ecosystem. Quantifying its impacts, however, is difficult due to the uncertainties in estimating the strength and variations of volcanic emissions. Here we developed and evaluated a new approach to combine satellite SO_2 detection and chemical transport modeling to assess the impact of the 2018 Mt. Kilauea eruption on air quality over Hawaii. During the sustained eruption of the Kilauea Volcano in Hawaii's Big Island from May to July 2018, considerable SO_2 and $PM_{2.5}$ enhancements were observed both from the ground and from space. We studied this case using an experimental version of the NOAA National Air Quality Forecast Capability (NAQFC) modeling system. Daily emissions of SO_2 and ash were estimated using a combination of SO_2 column density retrieved by Ozone Mapping and Profiling Suite (OMPS) Nadir-Mapper (NM) aboard the Suomi-NPP satellite and the NAQFC model with an inverse emission modeling approach. We found that the volcanic SO_2 emission rates peaked at 15,000 moles/s from the Kilauea's East Rift zone and Summit. The formation and transport of volcanic smog, or Vog, was highly dependent upon the vertical distribution of the volcanic emission, controlled by the heat flux of emission sources. We conducted four model simulations with various emission settings, and compared them to satellite data (CALIOP, OMPS and VIIRS) and in-situ measurements. All the runs tended to underpredict the peak values of surface SO_2 and $PM_{2.5}$ (particulate matter smaller than 2.5 micrometers in diameter). The "No Plume Rise" run underestimated the Vog plume rise and downstream transport. Using fixed emission rate or removing the temporal variations ("3-Day Mean") led to miss peak Vog effects or inconsistent

transport pattern compared to the observations. Therefore, the Base simulation with daily-varying emission and plume rise was used to quantify the air quality effects of the Kilauea eruption. We found that the volcanic eruption elevated surface $PM_{2.5}$ concentration by 30-40 $\mu g/m^3$ in the southeast part of the Big Island, with peak values up to 300 $\mu g/m^3$. The Vog effect on trace gases, such as O_3, NO_x, and non-methane hydrocarbons, were much weaker (<1 ppbV), but extended to the farther downstream.

Keywords: volcanic eruption, emission, air quality, SO_2, Hawaii

1. Introduction

There are eight major islands in the Hawaii State, and the Big Island (the largest) is located in the southernmost end of the island Chain. The Hawaii Big Island has the world's largest volcano Mauna Loa, whose recent eruption was in 1984. The Kilauea Volcano is the youngest volcano in the Hawaii's Big Island (Figure 1) and also one of the most active volcanos in the world. The Kilauea volcano erupted almost continuously from 1983 to 2018 (Patrick et al. 2019) with the largest eruption in the lower eastern rift zone beginning on 4 May 2018 (Neal et al. 2019). Ground swell, lava lake changes, and seismic activity in the weeks before the eruption caused the Hawaiian Volcano Observatory (HVO) to issue multiple warnings of possible volcanic activity beginning on 17 April 2018 and continuing until the eruption in early May (Neal et al. 2019). The eruption began with lava and SO_2 emanating from fissures within the Eastern Rift Zone (ERZ) (fissures in Figure 1), and progressed over the month of May to lava fountain eruptions from new fissure openings further downrift in the ERZ (Neal et al, 2019; Patrick et al, 2019; Vernier et al, 2019). Simultaneous to the eruptive activity within the ERZ, at the Kilauea summit, the lava lake level dropped, the summit wall began to collapse and a mixture of ash and SO_2 were ejected (Neal et al. 2019; Patrick et al, 2019). The eruption finally terminated in early August, two months after the eruption began (Neal et al. 2019).

From May to August 2018, the Kilauea volcano had a sustained eruption, emitting a large amount of lava, ash, and gases that were transformed into volcanic fog, or Vog. The volcanic emissions originated from two major sources: lava lake explosions and subsequent collapse of the Halema'uma'u crater within the Kilauea Summit (19.41ºN, -155.28ºW with an elevation of 1247 meter above sea level), and multiple fissures within the East Rift Zone where the lava outflow formed a lava river toward the Pacific Ocean (Figure 1) (Neal et al, 2019). The lava from these two areas came from the same lava reservoir under Mt. Kilauea (Pietruszka and Garcia, 1999; Thordarson and Garcia, 2018), and lava temperature in the tubes was about 1250°C. The East Rift Zone was the major lava outflow area during this event, and the lava outflow volume was about 145 million cubic meters in the first 47 days of eruption according to the USGS's Hawaiian Volcano Observatory (https://www.staradvertiser.com/2018/06/20/hawaii-news/lava-output-far-outpaces-previous-eruptions .

The vast amount of ash and trace gases emitted during the volcanic eruptions impose substantial impacts on the surrounding air quality and the ecosystem. Quantifying the air quality impacts of volcano eruptions, however, is difficult due in large to the uncertainties in estimating the strength and variations of volcanic emissions. In this study, we use a satellite-based emission inverse modeling approach to estimate volcanic emissions during the Kilauea Eruption. The inverse modeling has been widely used to refer emission. This method generally combines an inverse model with in-situ or satellite observations to adjust *a prior* model emission rate estimates to best match observations. Chai et al (2017) used HYSPLIT, a Lagrangian dispersion model, and MODIS observations to determine the source parameters for volcanic ash from the 2008 Kasatochi eruption. Resler et al (2010) used a CMAQ adjoint model with a 4D-Var approach to adjust the temporal variations of nitrogen dioxide emissions. Wang et al (2016) used an ensemble optimal interpolation method to adjust the black carbon emission and yielded significant improvement for black carbon prediction. Brunner et al. (2017) tested four Lagrangian inverse modeling systems with various inversion methods, such as Bayesian and extended Kalman Filter, to estimate the Hydrofluorocarbons emission over Europe. Since their inverse modeling simulations were driven by the same or similar meteorology (ECMWF and UK Met Office analyses), comparable results were produced by different ensemble members. Besides the inverse algorithms and certain assumptions, inverse modeling could be sensitive to a number of factors that affect the transport processes, including but not limited to the meteorology fields, emission characteristics, receptor types, and physical schemes in the transport/dispersion model. It should be noted that some of the aforementioned methods, such as 4D-Var, could consume a significant amount of computing resources. For the species actively involved in chemical reactions, the treatment could be even more complex and costly.

Here we implemented an inverse emission approach within a comprehensive air quality forecasting system using a whole-domain source-receptor relationship as the first-order approximation. Lamsal et al. (2011) showed an example of this approach: first, they set up the two forward model runs with first-guess emission and the emission perturbed by 15%, and then applied the emission-concentration relationship from the model runs with Ozone Monitoring Instrument (OMI) NO_2 data to adjust first-guess anthropogenic NO_x emission. A similar approach has been utilized by Stohl et al. (2011) to investigate the 2010 eruption of volcano Eyjafjallajökulli (Iceland), and they successfully reproduced the major features of the volcanic ash observations using a Lagrangian dispersion model constrained by satellite data. In this study, we employed a similar approach for the Kilauea Volcano eruption event to invert the emission from satellite observations. In our approach, the receptor is not at a specific location or over an area, but the entire model domain. This approach aimed to reduce uncertainty or variability of the inversed results, which were sensitive to the various model factors, such as transport, diffusion, and chemical transformation.

2. Methods and Settings

In this study of the 2018 Kilauea eruption, we employed an experimental version of the National Air Quality Forecast Capability (NAQFC) modeling system over Hawaii. The operational NAQFC is running 4 cycles per day initialized at 00, 06, 12, 18 UTC over Contiguous United States, Hawaii and Alaska domains. In this study, we ran CMAQ one cycle (12UTC) per day, and each run used the output of the previous run as its initial condition. The NAQFC's Hawaii domain covers all Hawaii islands with a 12km horizontal resolution and 22 vertical layers up to 100hPa. The chemical transport model is the Community Multiscale Air Quality (CMAQ) version 5.0.2 driven by the meteorological forecast from the North American Meteorological model (NAM) (Lee et al., 2017). The NAM meteorology is re-initialized at 12 UTC with NAM Data Assimilation System (NDAS). Anthropogenic emissions were based on National Emission Inventories (NEI2005). Biogenic emissions were calculated from the Biogenic Emission Inventory System (BEIS) 3.1.4. During the study period, the dominant source was the Kilauea volcanic emission, which, however, was hard to quantify. There were some in-situ measurements for SO_2 concentrations with sporadic spatial coverage, which could be useful to verify model results, but hardly used for estimating the total volcanic emission. In order to achieve the whole-picture view, the satellite data is employed to constrain the volcanic emission.

2.1 Volcano Emission Estimation

We used satellite data and a chemical transport model to estimate the volcanic SO_2 emission. The Ozone Mapping and Profiler Suite (OMPS) instrument aboard on the Suomi National Polar-orbiting Partnership (SNPP) satellites is originally designed to detect atmospheric ozone using ultraviolet (UV) band (Flynn et al, 2014). Besides its ozone products, the hyper-spectral UV satellite sensors, like OMPS-Nadir Mapper (NM) on SNPP, can provide daily global observations that are sensitive enough to measure atmospheric trace gases, including SO_2, down to the planetary boundary layer (Yang et al, 2013). In this study, the OMPS-NM total column SO_2 product is used to constrain the SO_2 emission. It should be noted that OMPS SO_2 total column reflects the SO_2 concentration's column loading, and is not directly associated with the volcanic SO_2 emission. To link the satellite column concentration mass loading with the emission, we used a chemical-transport model to identify the emission-concentration sensitivity:

$$\frac{dC}{dt} = \vec{V} \cdot \nabla C + C_{diff} + C_{dep} + C_{chem} + E, \qquad (1)$$

where C represents the SO_2 concentration and $\vec{V} \cdot \nabla C$ is the 3-D advection term of the SO_2 concentration. C_{diff}, C_{dep}, and C_{chem} are the diffusion, deposition (dry and wet), and chemical transformation terms that determine concentration changes, respectively. E is the emission term. We integrate these terms over a 3-D space in the Hawaii domain:

$$\iiint \frac{dC}{dt} dxdydz = \iiint \left(\vec{V} \cdot \nabla C + C_{diff} + C_{dep} + C_{chem} + E\right) dxdydz \quad (2)$$

Assuming the concentration is at pseudo equilibrium during one day over a certain area, e.g. Hawaii and the surrounding region, we then have:

$$\iiint -\left(\vec{V}\cdot\nabla C + C_{diff} + C_{dep} + C_{chem}\right)dxdydz = \iiint E dxdydz \quad (3)$$

Since the volcano emission is an isolated source, there was no upstream advection contribution toward the Hawaii region, and pollutant recirculation can be omitted when making regional 3-D integration. Therefore, both the $\vec{V}\cdot\nabla C$ and the C_{diff} terms contribute to the reduction of regional total SO_2 concentration, as well as the C_{dep} and the C_{chem} *terms*. The main gaseous chemical reaction of SO_2 is its reaction with OH radicals in CMAQ's CB05 mechanism. Other SO_2 chemical reactions, such as the heterogeneous formation of SO_2 to sulfate radical, also contribute to SO_2 loss as well. Within this self-contained system and by continuity we can make a first-order approximation:

$$\iiint -\left(\vec{V}\cdot\nabla C + C_{diff} + C_{dep} + C_{chem}\right)dxdydz \approx MC_{total} \quad (4)$$

where C_{total} is the regional total column loading and M is a constant representing the regional total SO_2 loss rate due to advection, diffusion, deposition and chemical transformation. Thus we have:

$$C_{total} \propto \iiint E dxdydz \quad (5)$$

Subsequently, the regional total column SO_2 is proportional to regional SO_2 emission, dominated by the Kilauea volcanic SO_2 flux during this event. With this relationship, we performed daily forward run of the air quality model with an initial estimated emission, then adjusted this emission proportionally to reduce the difference between model-simulated and OMPS-observed regional total SO_2 loadings. Since SO_2 is short-lived species (Lee et al, 2011), we omitted the effect of the residual SO_2 from the previous day and assumed that the regional total SO_2 loading reached a steady state daily. The SNPP satellite overpassed Hawaii daily around 23UTC and the OMPS took the snapshots of the spatial distributions, from which the total loadings of SO_2 were calculated. We assumed that the Kilauea volcanic SO_2 emission was at a constant rate for a given day during the study period.

Figure 2 showed the total SO_2 emission using this method starting from May to August 2018, during which elevated volcanic SO_2 was observed by the OMPS over Hawaii and the surrounding area. The sustained eruption lasted about four months and peaked around middle June. The temporal variations of SO_2 emission estimated from this method agreed well with the information from public reports about this eruption (https://en.wikipedia.org/wiki/2018_lower_Puna_eruption). Figure 2 also showed the whole-period mean SO_2 emission around 500 moles/s. To investigate the impact of the temporal variations of the volcano emissions on air quality, three sensitivity simulations were designed using 1) daily emission (Base) case; 2) a Whole-Period Mean (WPM) emission case; and 3) a 3-

day mean emission case. The first case used the emission rate derived from OMPS-NM daily observations, and the second case use a constant emission rate of 500 moles/s for the entire simulation period. The third run, using the 3-day mean method, retained some temporal variations but not as frequently as the Base run. One motivation of these time-averaging sensitivity runs was to emulate the operational environment, which tended to use static volcanic emissions. Since the volcano emission was the dominated SO_2 source during this event, we assumed that all these SO_2 loadings attributed to the surface flux were emitted from the Kilauea Volcano, and that the other sources, such as anthropogenic SO_2 emission, were much lower. The two lava outflow areas in the Kilauea Volcano, the Summit and ERZ, were supplied with the same lava source from the underground reservoir, and their outflow intensities were driven by the same underground lava pressure. Therefore, we assumed that their SO_2 emissions were proportionally correlated. During the study period, the ERZ was the major lava outflow area, where the poured-out lava formed a lava river flowing to the Pacific Ocean. At the lava lake of the Kilauea summit, the fresh lava flowed up, released volcanic pollutants, cooled and sank down, forming an up-and-down lava circulation. In our 12km Hawaii domain, the ERZ and summit were in two adjacent grids, and we set the summit SO_2 emission rate equal to one-tenth of that in ERZ.

Besides SO_2, the volcano also emitted ashes. At the Summit lava lake, the ash emission rate of ash was set to be 1.7% (mass ratio) of the corresponding SO_2 emission rate. For the ERZ area, the lava river had a higher ash emission rate as the high-temperature lava burned combustible materials at places it reached, such as grass, trees, roads, and buildings, leading to additional smoke emissions from those flamed and smoldering burns areas. We set the ash emission rate at ERZ is 86% (mass ratio) of the corresponding SO_2 emission at ERZ. This emission ratio was estimated based on the surface concentration monitoring (EPA Air Quality System network) for SO_2 and $PM_{2.5}$ (particle matter with diameter < 2.5 μm), and all the ash emissions entered the CMAQ air quality model as the species "PM Other" (PMOTHR, unspeciated component), which was mainly allocated into the accumulation mode in CMAQ's Aero6 mechanism.

2.2 Plume Rise and Lava Heat Flux

The volcano emissions were treated as point sources in CMAQ, similar to the typical treatment of wildfire emissions (Pouliot et al, 2005). The vertical distribution of wildfire or volcanic plume, including SO_2 and ash particles as constituents, was determined using the Briggs plume rise algorithm (Briggs, 1969), with the heat flux and heated area, as illustrated by Pouliot et al (2005) in the calculation of wildfire plume rise. The buoyancy flux F (in m^4/s^2) is proportional to the heat flux Q (in BTU/hr)

$$F = Q * 0.00000258 \quad (6)$$

Since not all emissions are available for plume rise, Pouliot et al. (2005) introduced the empirical buoyant efficiency (BE_{size}) to represent the fraction of wildfire emission available for rising plumes or the layers between the plume bottom and plume top

$$BE_{size} = 0.0703 * \ln(acres) + 0.3 \quad (7)$$

where *acres* is the fire size in acres. It means that the bigger an area is burned, a higher fraction of the plume will enter the elevated layers for plume rise. We adopted this approach and fed the lava heat flux to CMAQ for the Vog plume rise. The lava lake area at the summit was near-constant (~ 34 acres), while the area of ERZ's lava river varied from day to day, with an average size of around 800 acres. The lava heat flux depended on the lava outflow rate, temperature, and cooling speed. Carling et al. (2015) reported that the maximum brightness temperature in the open channel of the lava stream of Kilauea Volcano was 1,230°C, with some areas reaching 1,272°C. These temperature measurements, though taken in 2011, were used to specify the lava temperature in this study, since the lava physical characteristics likely remained unchanged over the years. The initial lava outflow temperature thus was set at 1250°C for the May-June 2018 eruptions at the Kilauea Volcano, and is relatively consistent with the lava temperature for this event as detailed in Gansecki (2019) and corroborated in Oppenheimer (2018). The Kilauea lava is basaltic (Gansecki et al. 2019; Patrick et al. 2019; Oppenheimer et al. 2018)), and its heat capacity is about 1000 J/kg/C for liquid phase and 1400 J/kg/C for solid phase.. The lava latent heat of fusion is about 400000 J/kg at melting point 1200°C (Patrick et al., 2004). Assuming that Kilauea lava finally cools to the ambient temperature of 30°C, its released heat rate would be 2.088×10^6 J/kg. The cooling time of lava could be quite long, but most heat was released during the early stages of the cooling process (Patrick et al, 2004). We therefore approximated the lava cooling with a simplified treatment, in which the lava mass released all its heat within one hour after leaving the open channel of the volcano. The lava outflow rate was estimated to be 145 million cubic meters in the first 47 days of eruption according to the USGS's Hawaiian Volcano Observatory (https://www.staradvertiser.com/2018/06/20/hawaii-news/lava-output-far-outpaces-previous-eruptions). Given this lava outflow rate, the SO_2 emission rate (from lava mass) was estimated to be 1.2 g/kg, as shown in Figure 2. This ratio was used to estimate the daily lava mass outflow rate in the ERZ area. At the summit of the Kilauea Volcano, the circulation of the lava lake was driven by the pressure of the lava reservoir from beneath, which also drove the lava outflow in the ERZ area. Therefore we assumed that the heat flux from the lava lake was proportional to the lava river in the ERZ area with a ratio of 4.2%, the same as their area ratio. During this study period, the Kilauea Volcano eruption was mostly effusive and the plume exit velocity was low. Consequently the VOG plume rise was mostly driven by its buoyancy from the lava heat flux. To evaluate the impact of the plume rise due to lava heat flux, we conducted a run without lava heat flux, or "No Plume Rise". In the next section, we discuss the results from the 4 runs mentioned above with a focus on the impact of the emission plume rise.

3. Result and Discussion

In this study, we relied on the *a priori* knowledge to estimate volcano emission to fill the gap of limited on-site information. Thus the emission variation and the associated heat flux derived from the daily OMPS SO_2 data were subject to uncertainties. To verify the emission estimation and the

corresponding model performance, we compared the simulated concentrations with the satellite retrievals and available in-situ observations.

3.1 Evaluation of Plume Rise Estimate with CALIOP Data

First, we examined how well the plume rise algorithm works to represent the vertical profile of the volcanic plume, using the aerosol profile data from the Cloud-Aerosol Lidar with Orthogonal Polarization (CALIOP) lidar aboard the CALIPSO satellite. CALIOP detects aerosol optical extinction coefficient (AOE) at 1064nm wavelength. Based on that, we derived the AOE at 532nm assuming the Vog has an Angström exponent about 1 (Sellitto, et al., 2018). CALIOP data had several overpasses near the Big Island of Hawaii during the eruptions, but none of its footprints directly intersected the ERZ, the major lava outflow zone. Figure 3a shows the total aerosol optical depth (AOD) from the CALIOP when it flew over the Big Island on May 23, 2018. The CALIOP data displayed two elevated profiles with high AOE values, around latitudes 18.8°N and 17.7°N, respectively. The high AOE profile at 18.8°N, located just south of the high terrain, extended from the surface (1000hPa) to 800hPa, and high AOE profile at 17.7°N was slightly lower. The CMAQ AOE was calculated with the reconstruction method (Binkowski and Roselle, 2003) from the aerosol mass concentrations.

Both the Base run and "No Plume Rise" (NPR) run underestimated the AOE. The NPR run showed the elevated high AOE (> 0.1) around 800hPa at 18°N, which was missed by the Base run. The Base run captured the elevated high AOE at 17.7°N but slightly overestimated the plume's height. On June 24 (Figure 4), the CALIOP had another similar overpass over the Big Island and showed the high AOE profile above 800hPa at the south edge of the big terrain. For this overpass, the Base run well captured the high AOE's height and location, though underestimated its intensity.

On July 3, CALIOP overpassed the nearby of the Big Island (Figure 5) and detected the elevated AOE above 600hPa around 18°N. Both Base and NPR runs showed that elevated AOE, but the Base run had higher AOE (>0.03) existed while the AOE of NPR run was always < 0.02 for the heights above 600hPa. Since the spatial and temporal coverage of CALIOP data was relatively limited, the difference between Base and NPR runs was not very significant for the CALIOP comparison.

In these three scenarios of comparison to the CALIOP satellite Lidar data, the two runs showed some differences, due to their different treatments of volcanic emission's vertical distribution: with and without emission plume rise. Comparing to the NPR run that simply put all volcanic emissions into the lowest model layer, the Base run showed more agreements with the CALIOP for the aerosol spatial distribution pattern, though the both runs had much lower AOE than the CALIOP product. Even though the difference between these two runs sometimes were not significant due to the limited CALIOP temporal and spatial coverage, the existing scenarios still indicates that the

Base run with plume-risen volcanic emissions driven by the lava heat flux yielded results more reasonable than that without plume rise.

3.2 Effects of emission configuration on SO_2 simulation: a comparison against OMPS SO_2

Figures 6-8 showed the effects of different emission configuration on SO_2 column density simulated by CMAQ. Here we compared the OMPS SO_2 total-column retrieval data against four CMAQ simulations: Base with daily emissions and Briggs plume rise with estimated heat input, No Plume Rise, Whole-Period Mean (WPM) emission, and 3-day Mean (3DM) emissions, on 05/23, 06/24 and 07/03 respectively. The CMAQ SO_2 columns were calculated with the corresponding OMPS retrieval averaging kernels. The OMPS SO_2 domain used to estimate the daily volcano emission over the Hawaii surrounding region, was displayed in Figure 6, along with the model results and the NAQFC Hawaii domain. The original OMPS retrieval was based on several prescribed vertical profiles (Yang et al., 2013 and Yang, 2017). The OMPS-NM SO_2 retrievals included several kinds of prescribed tropospheric profiles, and what we used here was based on the lower-Tropospheric profile since the major injection height of volcano plume was in the lower troposphere. We chose the 23UTC CMAQ result to compare, as it was closest to the OMPS overpass time. The resolution of OMPS SO_2 from the SNPP satellite was about 50km, which was coarser than the 12km CMAQ model resolution.

All the model results showed overall consistent SO_2 column loadings and transport patterns with the OMPS retrieval during that date when the satellite retrievals were available over the Hawaii region. However, there were also some differences. The model results showed all the SO_2 peak loadings over the source region, and it faded away as the volcanic plume moved downstream. The satellite product showed the overall similar pattern but had location shifts, e.g. the OMPS SO_2 on 05/23 and 06/24 had their peak values displaced from the emission area. It also had some sporadic and isolated middle-range spots ($SO_2 \sim 0.5$-1 DU) outside the plume covered region. Some of these issues could be related to the retrieval quality or OMPS detection limit. Another possible cause was the temporal variation of the volcanic SO_2 emission. In this study, the volcano emission was kept unchanged for each day. However, in real world, the emission could have temporal variation during the course of a day. For instance, on May 23, all the model results showed two major Vog zones where the highest SO_2 loading (SO_2 loading > 2 DU) was around the volcano and the further downwind plume was much weaker with SO_2 < 5DU due to the plume diffusion, dilution or decaying, as we assumed that the volcano emission did not change in 24 hours. The OMPS SO_2 had a similar pattern, but the SO_2 loading in the further downwind was not weaker (Figure 6a), implying that the plume in the further downwind could be caused by stronger emissions at earlier times. The once-per-day snapshot might not be sufficient to fully capture the emission variations.

The four model runs also showed some differences among these three perturbation scenarios. The 3DM and WPM runs had similar emissions on May 23, higher than the Base run (Figure 2), which resulted in their difference in Figure 6, and the Base run (Figure 6b) had a smaller area with SO_2 > 2DU than the WPM (Figure 6d) and 3DM (Figure 6d) runs. Without the daily-varying emission,

the WPM and 3DM runs yielded continuous SO_2 outflow patterns, unlike the Base run's two-zone pattern for high SO_2 loading (figure 6b). The No Plume Rise run had the smallest high SO_2 area among these four runs, as turning off the heat flux or plume rise limited the upward transport of the volcano plume and emitted SO_2 was relatively quickly deposited back to surface. Due to its relatively higher wind speed, the downstream transport in the elevated layer is usually quicker than that near the surface. So, the NPR run also had a relatively limited downstream extension. For the May 23 scenario, the Base run was more consistent with the OMPS SO_2 retrievals than the other three runs.

Figure 7 showed the similar plot but for the date of June 24, 2018 when the base emission was higher than the WPM and 3DM. Among these four simulations, only the Base run showed the two-zone pattern with SO_2 DU > 5, while the OMPS retrievals showed the two-zone pattern with SO_2 DU > 20. Although all the runs underestimated the SO_2 column loading, the Base run was better than the rest 3 runs. The WPM showed the most significant underestimation, due to its lowest volcanic SO_2 emission on June 24. Figure 8 shows a similar story for July 3, 2018 in which the changed wind direction caused a different transport pattern, agreed with all the model runs. Although all of them had the similar SO_2 loading over the big island, the Base run showed stronger downstream hot spot with SO_2 DU >2 and the stronger northeastward arm extended from the Big Island, and all the rest of the runs underestimated more.

The OMPS SO_2 data had relatively broad spatial coverage, which helped for the comparisons of the spatial patterns. The NPR run underestimated the Vog plume rise and downstream transport. The WMP with constant emission rate or 3DM that removes the temporal variations missed the peak Vog events or inconsistent transport pattern compared to the OMPS SO_2 retrievals. The Base run showed results that are more reasonable than the other runs.

3.3 Comparison to VIIRS AOD

Aboard on the same satellite (SNPP), there was another instrument, Visible Infrared Imaging Radiometer Suite (VIIRS), from which the aerosol optical depth (AOD) could be retrieved. Figure 9 shows the comparison of CMAQ AOD to the VIIRS AOD product on June 25 when the Hawaii surrounding area was largely uncovered from clouds and the retrieval was available during the SNPP-VIIRS overpass time. The CMAQ AOD was obtained using the reconstruction method (Binkowski and Roselle, 2003) which used the mass concentrations of aerosol chemical compositions to calculate the total aerosol extinguish efficient with a look-up table.

In general, the CMAQ AOD showed a smaller value for the background than that in VIIRS retrievals, as we used clean lateral boundary conditions in this study, which might have caused a low bias for aerosol prediction. All the runs captured the major transport patterns. Unlike the SO_2 being concentrated near the source area, the AOD peak value might not be in the volcano source area, shown by the VIIRS retrieval, since the SO_2 formation to sulfate could take some time. Similar to the previous comparison to OMPS SO_2, the Base run has broader downstream high

AOD zone (AOD > 0.5) (Figure 9b), while the other runs displayed more severe underprediction due either to insufficient plume rise (No Plume Rise run, Figure 9c) or to lower volcanic emission (WPM, Figure 9d).

This result is consistent with the comparison to OMPS-NM SO_2, and the Base run yielded better result with the right reason. During the 2018 Kilauea eruption, the volcanic emission showed strong temporal variation, and omitting that variation resulted in the underestimated peak emission in the WPM run. The emission plume rise was important, and affected not only the volcanic emission's vertical distribution, but also its horizontal transport pattern as the upper layer usually had higher wind speed. NPR put all volcanic emission near surface, which also resulted in excessive dry deposition loss of Vog.

Figure 10 shows the sulfate fraction in total AOD in the Base run on two selected dates: May 16 at the beginning of the Kilauea volcano eruption, and May 30 when the eruption was ongoing. When the eruption just started, AOD was not very high except in the source region where the volcanic ash was the dominant AOD contributor, and sulfate AOD came mainly from the background as sulfate formation needed some times. On the latter date, sulfate was the dominant aerosol except near the source region, where volcano ash could be major aerosols. Since the SO_2 was the major pollutant from the eruption of the Kilauea Volcano and the sulfate is the final fate of most SO_2, it was not surprising that the sulfate portion in total aerosol spread widely in the downwind area of this relatively clean region. Sulfate was usually in the ultrafine particle (Aitken mode), or accumulated mode, which stayed longer in the atmosphere than the coarse aerosols. So, in the downwind area, the sulfate portion became higher.

3.4 Comparisons against SO_2 Profile Measurements

During this eruption, a research team from the University of Houston measured the SO_2 profile concentrations over the Southwestern corner of the Big Island (the location of "June launches" in Figure 1). We compared the model results with these in-situ measurements, shown in Figure 11. These profiles were measured near the local noon over the Island, when the PBL convection was relatively strong.

During the first scenario at 00UTC on June 22, the observations showed SO_2 concentration (~ 100 ppbv) peaked at an altitude of about 1.5km above sea level. The elevated SO_2 values were transported horizontally from the source region, then descended and mixed down to the surface. All the runs showed a similar pattern, but underestimated the 1.5km high values and overestimated surface SO_2 concentrations. All the runs had the overmixing issue, bringing too much SO_2 to the surface while diluting the peak concentrations at 1.5km level. The NPR run had the highest SO_2 concentration, the closest to the observations at the elevated level, but it also yielded the highest overprediction near the surface. The altitude of Kilauea Summit was about 1.2km above sea level, which was very near to the altitude of peak SO_2. The horizontal transport could bring the surface SO_2 from the summit to the observation location, as the NPR run put all the emissions near the

surface, and had the highest near-surface SO_2 concentrations among all the runs. The WPM and 3DM had lower emissions, which resulted in lower SO_2 concentrations (Figure 11a).

Figure 11b showed another profile measurement launched 2 hours later, in which the Base run had similar but slightly higher near-surface concentrations than the NPR run, and yielded a much higher peak SO_2 concentrations at 0.5 km and 1km. This SO_2 peak was transported from the ERZ source region through recirculation. Due to the overprediction of PBL height in these runs, all the runs overmixed the SO_2 into the higher-than-actual altitude at ERZ and led to overpredicting the SO_2 peak height at the observation location. In this scenario, the WPM run had better agreement with the observation.

Figure 11c showed the SO_2 profile comparison two days later, and the measured SO_2 peak concentrations appeared near the surface and dropped quickly at higher altitudes. It implied that the transport from the Volcano source region to the observation location was mainly through low altitudes. All the runs overpredicted the vertical mixing again and had relatively uniform vertical profiles from the surface to the altitude of 2km. The NPR run had the highest overprediction during the scenario due to its higher near-surface SO_2 concentrations.

All the observed profiles for the three scenarios showed second SO_2 peak concentrations around or above 3km, missed by all the runs. It implied that Vog emission and transport could have more complex features, which were not well captured by the models, due to the uncertainties in emission and meteorology, or insufficient temporal/spatial resolutions.

3.5 Model Performance in Predicting Surface Concentrations

The major health consequence of volcano eruptions is elevated concentrations of air pollution at nose level. In this section, we evaluated how well each model setup predicted surface concentrations of SO_2 and $PM_{2.5}$. During this eruption period, U.S. EPA Air Quality System (AQS) monitoring stations recorded hourly surface concentrations (Whitty et al., 2020).

Figure 12 showed the simulations compared to surface in-situ measured SO_2 and $PM_{2.5}$ at three U.S. EPA AQS stations. Among them, the Pahala station was the nearest station to the Kilauea Summit, and it recorded short-duration (< 12 hours) peaks with SO_2 mixing ratio > 600ppbV during this eruption event. The models could not capture some of these Vog peaks due to its limited spatial resolution (12km) and emission's temporal resolution (daily) (Figure 12a). Among these simulations, the No Plume Rise run yielded the highest SO_2 and $PM_{2.5}$ concentrations as its volcanic emissions were put near the surface, which caused overprediction, especially for the period of June 15-25 and July 1-15 (for $PM_{2.5}$, Figure 12b). It also had the worst correlation coefficient and RMSE (Figure 12a,b) for both SO_2 and $PM_{2.5}$ over that station. The run with whole-period mean emission had the highest correlation coefficient for SO_2 comparison, but underestimated most SO_2 peaks. The 3DM run did better as it retained some temporal variations of emissions.

Figure 12c,d showed a similar comparison over the Ocean View station, southwestern Big Island, which was near the "June launch" place for SO_2 profile measurement. All the runs missed the major SO_2 peaks on May 22, May 28-31 and June 12-23. The NPR run still yielded higher $PM_{2.5}$ than the other runs (Figure 12d), and its SO_2 prediction did not show that high values. The SO_2 prediction from the NPR run was lower than that from the Base run for most times over the Ocean View station, which was not near the source area. So, the high surface SO_2 concentration near source region in the NPR run did not yield the corresponding high concentration over the downstream area, implying that the transport pattern became more important and the low-altitude transport was not as efficient as elevated transport. Over this station, the NPR run also had the lowest correlation coefficient for SO_2 and $PM_{2.5}$. Some of these observed SO_2 spikes at Ocean View station exceeded 1000 ppbv, which was even higher than those spikes at the Pahala station, suggesting that the distance from the source area might not be the dominant factor for the SO_2 concentration, and the transport factor could play a more important role under certain circumstances.

The Kona station lies in the western Big Island and is the farthest station from the Mt. Kilauea Summit among these three. All the models missed the major SO_2 peaks on May 22, May 28-June 1, June 15-25 and after July 1 at Kona (Figures 12e and 12f). Our analysis indicated that the underprediction was due in part to the biases in the wind fields, especially near the surface, as some complex terrains existed in the Hawaii Big Island and the 12km NAM near-surface wind field had some biases. The NPR run turned out to yield lower SO_2 and $PM_{2.5}$ concentrations than the Base run, which further confirmed that the Vog transport pattern became more important for the downstream region, as the high near-surface $SO_2/PM_{2.5}$ concentrations of NPR run near the source area did not produce the corresponding higher $SO_2/PM_{2.5}$ concentrations in the downstream area.

In this surface comparison, the model-observation correlations were relatively low, even near the source area, implying that there could be some unknown volcanic emission variation, not captured by the daily OMPS SO_2 constrained emission. Over the further downstream area, the meteorological and associated transport factor could play a more important role for the predictions. Among these 4 runs, the NPR run tended to overpredict $SO_2/PM_{2.5}$ with highest RMSE near the source area, and had the lowest correlation coefficients over two stations; the 3DM run had the lowest correlation coefficients over the Kona station; the WPM run missed all the peak values and had the systematic underpredicting bias over these stations. The Base run had relatively more reasonable overall results, though it did not always score the best.

The surface station observation indicated that the major pollutant from this eruption was SO_2, but it also emitted ashes, which enhanced the surface $PM_{2.5}$. SO_2 formed sulfate also contributed to aerosols, especially in the downwind area. In this study, we assumed that the volcanic ash emission was proportional to the corresponding SO_2 emission as they were co-emitted from the same source. The surface observation over the Pahala station showed that this assumption was valid for some dates, e.g. 05/19-05/21 and 05/28-05/29. However, during some events, such as these on May 25

and May 31, the high $PM_{2.5}$ spikes (Figure 12b) were not associated with the corresponding SO_2 enhancements (Figure 12a), implying that there could be other aerosol sources, such as lava caused biomass burning that was not included in the model emission, or volcano ash emission was not always proportional to the SO_2 emission. In this study, we used the clean-background lateral boundary condition. If the background of Hawaii was not very clean due to trans-Pacific sources or ship emissions, our model underestimated the background aerosol concentration, especially over the downwind areas, e.g. Ocean View and Kona stations (Figures 12d, 12e).

3.6 Quantifying Air Quality Effects of the Kilauea Eruption

Analyses in the previous sessions indicated that the Base run, which was configured with daily emission and plume rise, produced overall better results. Therefore, this model simulation was used here to quantify the air quality effects of the Kilauea eruption. The volcanic pollutants emitted from the Mt. Kilauea significantly affected the atmospheric environment of Hawaii surrounding areas. Besides the immediate increases in SO_2, sulfate and total $PM_{2.5}$ concentrations, the volcanic eruption affected the entire photochemical process (von Glasow et al., 2009). Figure 13 showed a snapshot of predicted changes in after including the volcanic emissions, or difference between the Base run and a run without volcano emissions. The gaseous chemistry of SO_2 is relatively slow, mainly through reaction with OH radical. When the Kilauea Volcano emitted a large amount of SO_2, the OH concentration was reduced, which was also caused by the lower daytime photolysis rate due to the higher AOD loading. The OH reduction slowed down of almost all the atmospheric chemical reactions. One direct impact was the increases of NO_x and non-methane hydrocarbons (NMHC) over the source region and its downstream area (Figure 13a,c), by curbing the related reactions, such as NO + OH $\rightarrow$ HNO2, NO_2 + OH $\rightarrow$ HNO_3 and NMHC + OH $\rightarrow$ Products. The increase in sulfate acid in the air also changed the aerosol thermodynamic that decreased gas to particle conversion of the nitric acid (Nenes et al., 1998). The volcanic influence on O_3 is more complex. Near the volcano source region (Figure 13b), where there was few NOx and NMHC emissions, the reduction of photolysis rates and OH leads to O_3 increment by limiting O_3 photodissociation and the reaction of O_3 + OH $\rightarrow$ HO_2 + O_2, which represents the main O_3 consumption under the clean background. Over the western island where some anthropogenic and biogenic emissions existed, the reduction of photolysis rates and OH slowed down the photochemical production of O_3 and led to O_3 decrease. During nighttime (not shown), the volcanic SO_2 mainly led to reduced O_3 by increasing NO_x titration. The increased NO_x could also led to NMHC reduction over that area through the thermal reactions between them, such as NO_2+ISOPRENE, which is a slow reaction. So, the NMHC change due to the volcanic emission was mainly increments due to the lower OH (Figure 13c). Compared to the $PM_{2.5}$ increment (Figure 13d) caused by the volcanic eruption, all the changes on gaseous species other than SO_2 were relatively limited, around or less than order 0.1 ppbV in most areas. The maximum difference in this domain during this period is about 0.1 ppbV for NOx, 0.6 ppbV for O_3, and 0.8 ppbV C for NMHC.

Figure 14 showed the average and maximum effects of volcanic emissions on surface concentrations of $PM_{2.5}$, O_3, NO_x and VOCs during the study period over Hawaii. The eruption elevated surface $PM_{2.5}$ concentration by 30-40 $\mu g/m^3$ in the southeast part of the Big Island (Figure 14a), with peak values increased by up to 300 $\mu g/m^3$. The peak values were caused predominantly by primary emissions (ash). Across the southern Big Island and the west to the Island, surface $PM_{2.5}$ showed an increase between 10 and 20 $\mu g/m^3$ in the average concentration, and between 20-200 $\mu g/m^3$ in the maximum concentration. Compared to the large changes in $PM_{2.5}$, the effect on trace gases were much weaker. Volcanic emissions only slightly reduced surface O_3 by up to 0.15 ppbv in the central southern Island (Fig. 14c). There was a small perturbation, in both directions, across a large area further downwind, with the maximum change reaching up to 0.6 ppbv (Fig. 14d). The average changes of NO_x were mainly over the southern Big Island, while the maximum changes were found over Honolulu and downwind area, since the largest emission sources of NO_x in Hawaii were located in Honolulu and other cities on the island of Oahu. However, the change on NMHC did not show the similar spatial variations, as the OH concentration is main the controlling factor for NMHC oxidization (Fig. 14g, h).

4. Conclusion

In this study, we tested the method of using satellite retrievals and full-chemistry inverse modeling to quantify emissions from volcanic eruption and its effects on air quality. We used the SO_2 observations from OMPS-NM aboard the SNPP satellite to estimate the daily volcano emissions, including the SO_2, ashes, and heat flux during the 2018 Kilauea Volcano eruption. These inputs were used to drive the simulations of air quality effects over Hawaii using an experimental version of the National Air Quality Forecast Capability modeling system and the results were evaluated against a suite of ground and space observations. The model results generally agreed well with both satellite data and in-situ measurements over Hawaii Big Island, though short-lived peak values of SO_2 and $PM_{2.5}$ were not always captured. Some of the biases may be due to coarse temporal (e.g., daily volcanic emissions) and spatial resolutions (12km) in the meteorology and air quality models over complex terrain. The sulfate was the dominant aerosol component of the Vog plume in the areas downwind to the volcanic sources (Kilauea Summit and East Rift Zone).

Our results highlighted the key role of emission estimates and plume rise calculation in studying the air quality effects of volcanic eruption. We conducted three sensitivity studies without the lava heat flux or with temporal mean emissions. When turning off the lave heat flux, there was no plume rise and all volcanic emissions initially entered the atmosphere through the surface layer, which resulted in higher near-surface concentrations in the source region and limited downstream transport. The No Plume Rise run yielded higher biases in both near-source (over-prediction) and downstream (under-prediction) areas, and its transport pattern did not agree with satellite observations. Using static emissions and averaging emissions resulted in missing peak Vog effects or inconsistent transport pattern compared to the observations. Besides these factors, meteorological bias was another important issue for the predictions. During this study, the model

tended to overpredict the daytime vertical mixing over the Big Island, and this bias affected the vertical distribution of the Vog plumes.

Mt. Kilauea is an isolated source and SO_2 is relatively short-lived species, with few influences of upstream transport or pollutant recirculation. This helped to reduce the complexity of estimating the emission from the eruption using satellite retrieved SO_2. More work is needed for extending this method to estimate emissions in regions with more diverse high-density sources. The emission estimation approach based on the satellite retrievals available only once or twice per day cannot capture the full temporal variations and could miss significant emissions patterns. Higher-frequency observations would be helpful. Some discrepancies, such as satellite vs in-situ measurement, and SO_2 vs aerosol prediction biases, still need to be addressed in the future.

Code and Data availability

The source code used in this study is available online at https://github.com/NOAA-EMC/EMC_aqfs (last access: 4 May 2020; NOAA-EMC, 2020). The OMPS-NM SO_2 data are available in https://disc.gsfc.nasa.gov/datasets/OMPS_NPP_NMSO2_L2_2/summary. The U.S. EPA AQS data are in https://aqs.epa.gov/aqsweb/airdata/download_files.html. The CALIPSO satellite Lidar data are accessible through https://opendap.larc.nasa.gov/opendap/CALIPSO/LID_L2_05kmAPro-Standard-V4-20/2018/contents.html. The VIIRS AOD data used here are in ftp://ftp.star.nesdis.noaa.gov/pub/smcd/VIIRS_Aerosol/npp.viirs.aerosol.data/epsaot550/

Acknowledgement

The research was supported by NOAA National Air Quality Forecast Capability (grant # T8MWQAQ), NASA Health and Air Quality Program (grant # NNX16AQ19G) and the NOAA Joint Polar-orbiting Satellite System Program (grant # NA19NES4320002).

Reference:

Binkowski, F. S., and S. J. Roselle, (2003), Models-3 Community Multiscale Air Quality (CMAQ) model aerosol component: 1. Model description, J. *Geophys. Res., 108(D6), 4183, doi:10.1029/2001JD001409*.

Briggs, G. (1969), Plume rise, *Tech. Rep. Crit. Rev. Ser*. 81pp., Natl. Tech. Inf. Serv., Springfield, Va.

Brunner, D., Arnold, T., Henne, S., Manning, A., Thompson, R.L., Maione, M., O'Doherty, S. and Reimann, S., 2017. Comparison of four inverse modelling systems applied to the estimation of HFC-125, HFC-134a, and SF 6 emissions over Europe. *Atmospheric Chemistry and Physics*, 17(17), pp.10651-10674.

Byun D. and J. Ching, Ed. (1999); "Emission Subsystem", Science Algorithms of the EPA Models-3 Community Multiscale Air Quality (CMAQ) Modeling System, U.S. Environmental Protection Agency, Washington DC, 1999; EPA-600-R-99-030, pp.97-101.

Carling, G.T., Radebaugh, J., Saito, T., Lorenz, R.D., Dangerfield, A., Tingey, D.G., Keith, J.D., South, J.V., Lopes, R.M. and Diniega, S. (2015). Temperatures, thermal structure, and behavior of eruptions at Kilauea and Erta Ale volcanoes using a consumer digital camcorder. *Geo. Res. J.*, 5, pp.47-56. https://doi.org/10.1016/j.grj.2015.01.001

Flynn, L., C. Long, X. Wu, R. Evans, C. T. Beck, I. Petropavlovskikh, G. McConville, W. Yu, Z. Zhang, J. Niu, E. Beach, Y. Hao, C. Pan, B. Sen, M. Novicki, S. Zhou and C. Sefto (2014). Performance of the ozone mapping and profiler suite (OMPS) products. *J. Geophys. Res., Atmospheres*, 119(10): 6181-6195, doi:10.1002/2013JD020467.

Gansecki, C., R. L. Lee, T. Shea, S. P. Lundblad, K. Hon, C. Parcheta, (2019) The tangled take of Kilauea's 2018 eruption as told by geochemical monitoring. *Science*, 366, eaaz0147. doi: 10.1126/science.aaz0147.

Lamsal, L. N., R. V. Martin, A. Padmanabhan, A. van Donkelaar, Q. Zhang, C. E. Sioris, K. Chance, T. P. Kurosu, and M. J. Newchurch (2011), Application of satellite observations for timely updates to global anthropogenic NOx emission inventories, *Geophys. Res. Lett.*, 38, L05810, doi:10.1029/2010GL046476.

Lee, C., R. V. Martin, A. van Donkelaar, H. Lee, R. R. Dickerson, J. C. Hains, N. Krotkov, A. Richter, K. Vinnikov,and J. J. Schwab (2011), SO2 emissions and lifetimes: Estimates from inverse modeling using in situ and global, space-based(SCIAMACHY and OMI) observations,J. Geophys. Res.,116, D06304, doi:10.1029/2010JD014758

Lee, P., J. McQueen, I. Stajner, J. Huang, L. Pan, D. Tong, H.-C. Kim, Y. Tang, S. Kondragunta, and M. Ruminski, (2017). NAQFC developmental forecast guidance for fine particulate matter (PM2. 5), Weather and Forecasting, 32: 343-60. doi:10.1175/waf-d-15-0163.1.

Liu, C., T. Lay, and X. Xiong, (2018), Rupture in the 4 May 2018 MW6.9 earthquake seaward of the Kilauea East Rift Zone fissure eruption in Hawaii. Geophysical Research Letters, 45, 9508–9515. https://doi.org/10.1029/2018GL079349.

Nadeau, P.A., Werner, C.A., Waite, G.P., Carn, S.A., Brewer, I.D., Elias, T., Sutton, A.J. and Kern, C., (2015) Using SO_2 camera imagery and seismicity to examine degassing and gas accumulation at Kīlauea Volcano, May 2010. *Journal of Volcanology and Geothermal Research*, *300*, pp.70-80.

Neal, C. A., S. R. Brantley, L. Antolik, et al. (2019) The 2018 rift eruption and summit collapse of Kilauea volcano. *Science,* 363, 367-374. doi: 10.1126/science.aav7046

Nenes, A., Pandis, S.N. & Pilinis, C. ISORROPIA: A New Thermodynamic Equilibrium Model for Multiphase Multicomponent Inorganic Aerosols. *Aquatic Geochemistry* **4,** 123–152 (1998). https://doi.org/10.1023/A:1009604003981

Oppenheimer, C., B. Scaillet, A. Woods, A. J. Sutton, T. Elias, Y. Moussallam (2018) Influence of eruptive style on volcanic gas emission chemistry and temperature. *Nature Geoscience*. 11, 678-681. doi: 10.1038/s41561-018-0194-5.

Patrick, M. R., Dehn, J. and Dean, K. (2004). Numerical modeling of lava flow cooling applied to the 1997 Okmok eruption: Approach and analysis. *Journal of Geophysical Research: Solid Earth*, 109(B3). https://doi.org/10.1029/2003JB002537

Patrick, M. R., H. R. Dietterich, J. J. Lyons, A. K. Diefenbach, C. Parcheta, K. R. Anderson, A. Namiki, I. Sumita, B. Shiro, J. P. Kauahikaua (2019) Cyclic lava effusion during the 2018 eruption of Kilauea volcano. *Science*. 366, eaay9070. doi: 10.1126/science.aay9070.

Pietruszka, A. J. and Garcia, M. O. (1999), The size and shape of Kilauea Volcano's summit magma storage reservoir: a geochemical probe, Earth and Planetary Science Letters, Volume 167, Issues 3–4, 311-320, https://doi.org/10.1016/S0012-821X(99)00036-9.

Pouliot, G., Pierce, T., Benjey, W., O'Neill, S.M. and Ferguson, S.A. (2005), Wildfire emission modeling: integrating BlueSky and SMOKE. In the *14th Annual International Emission Inventory Conference* (pp. 11-14).

Resler, J., Eben, K., Jurus, P. and Liczki, J., 2010. Inverse modeling of emissions and their time profiles. Atmospheric Pollution Research, 1(4), pp.288-295.

Sellitto, P., Spampinato, L., Salerno, G. and La Spina, A., 2018. Aerosol Optical Properties of Pacaya Volcano Plume Measured with a Portable Sun-Photometer. Geosciences, 8(2), p.36.

Stohl, A., Prata, A.J., Eckhardt, S., Clarisse, L., Durant, A., Henne, S., Kristiansen, N.I., Minikin, A., Schumann, U., Seibert, P. and Stebel, K. (2011). Determination of time-and height-resolved volcanic ash emissions and their use for quantitative ash dispersion modeling: the 2010 Eyjafjallajökull eruption. Atmospheric Chemistry and Physics, 11(9), pp.4333-4351. https://doi.org/10.5194/acp-11-4333-2011

Thordarson, T. and Garcia, M. O. (2018), Variance of the flexure model predictions with rejuvenated volcanism at Kilauea Point, Kaua'i, Hawai'i. *Front. Earth Sci.* 6:121. doi: 10.3389/feart.2018.00121.

Vernier, J. P., L. Kalnajs, J. A. Diaz, T. Reese, E. Corrales, A. Alan, H. Vernier, L. Holland, A. Patel, N. Rastogi, F. Weinhold, S. Carn, N. Krotkov, J. Murray (2020), VolKilau: volcano rapid response balloon campaign during the 2018 Kilauea eruption. *Bull. Amer. Meteor. Soc*. doi: 10.1175/BAMS-D-19-0011.1.

von Glasow, R., Bobrowski, N. and Kern, C., 2009. The effects of volcanic eruptions on atmospheric chemistry. *Chemical Geology*, 263(1-4), pp.131-142. doi:10.1016/j.chemgeo.2008.08.020

Wang, P., Wang, H., Wang, Y.Q., Zhang, X.Y., Gong, S.L., Xue, M., Zhou, C.H., Liu, H.L., An, X.Q., Niu, T. and Cheng, Y.L., 2016. Inverse modeling of black carbon emissions over China using ensemble data assimilation. Atmospheric Chemistry and Physics, 16(2), pp.989-1002.

Wang, S.W., Zhang, Q., Streets, D.G., He, K.B., Martin, R.V., Lamsal, L.N., Chen, D., Lei, Y. and Lu, Z., 2012. Growth in NOx emissions from power plants in China: bottom-up estimates and satellite observations. Atmospheric Chemistry and Physics, 12(10), pp.4429-4447.

Whitty, R., E. Ilyinskaya, E. Mason, et al. (2020) Spatial and temporal variations in SO_2 and $PM_{2.5}$ levels around Kilauea volcano, Hawaii during 2017-2018. *Front. Earth Sci*. 8:36. doi: 10.3389/feart.2020.00036

Yang, K., R. R. Dickerson, S.A. Carn, C. Ge, and J. Wang, (2013). First observations of SO2 from the satellite Suomi NPP OMPS: Widespread air pollution events over China, *Geophys. Res. Letter.*, doi:10.1002/grl.50952.

Yang, K. (2017), OMPS-NPP L2 NM Sulfur Dioxide (SO_2) Total and Tropospheric Column swath orbital V2, Greenbelt, MD, USA, Goddard Earth Sciences Data and Information Services Center (GES DISC), https://doi.org/10.5067/A9O02ZH0J94R.

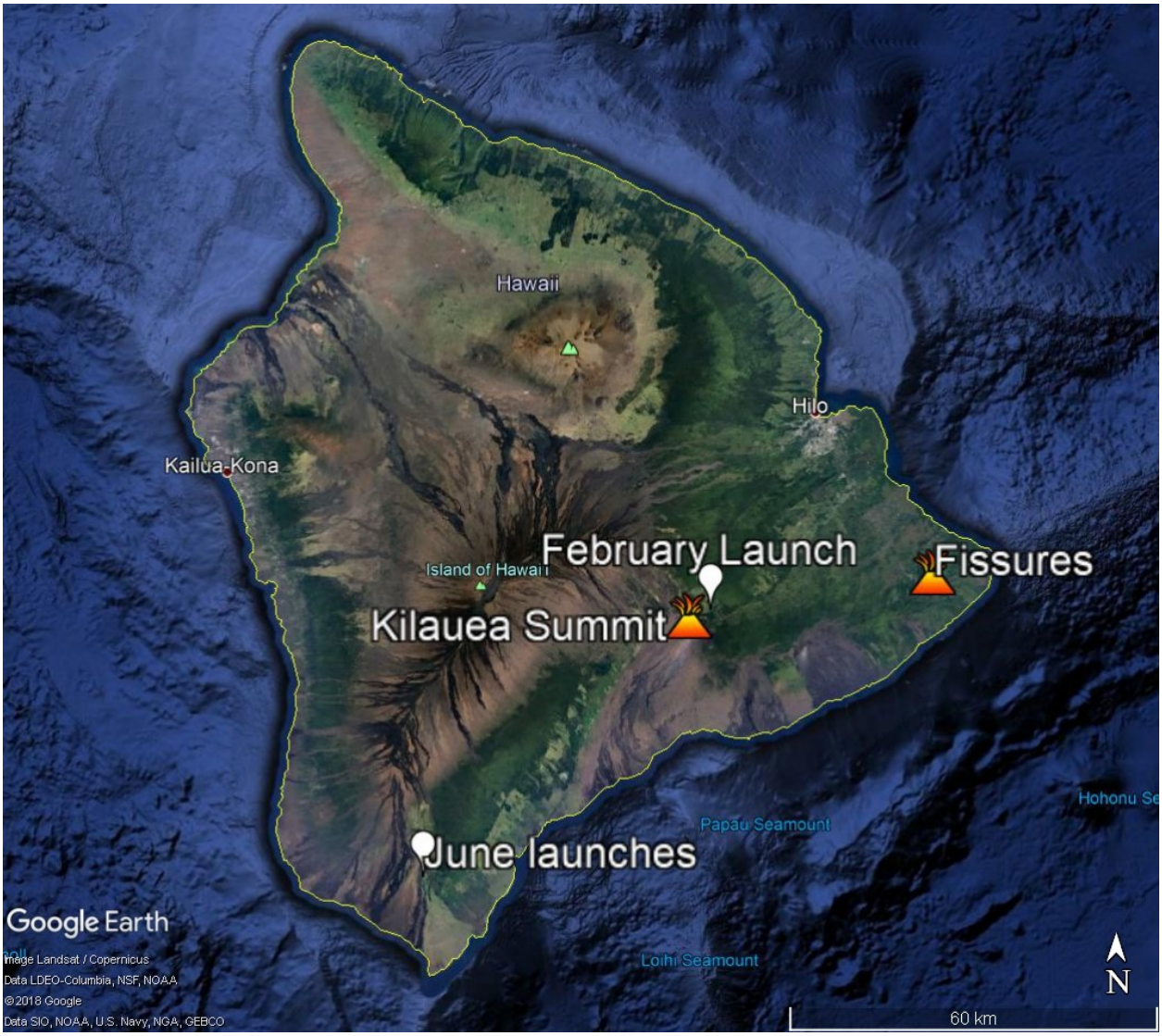

Figure 1. The map of big island of Hawaii, where the Kilauea Summit and East Rift Zone (marked as Fissures) are the major eruption areas during May-August, 2018.

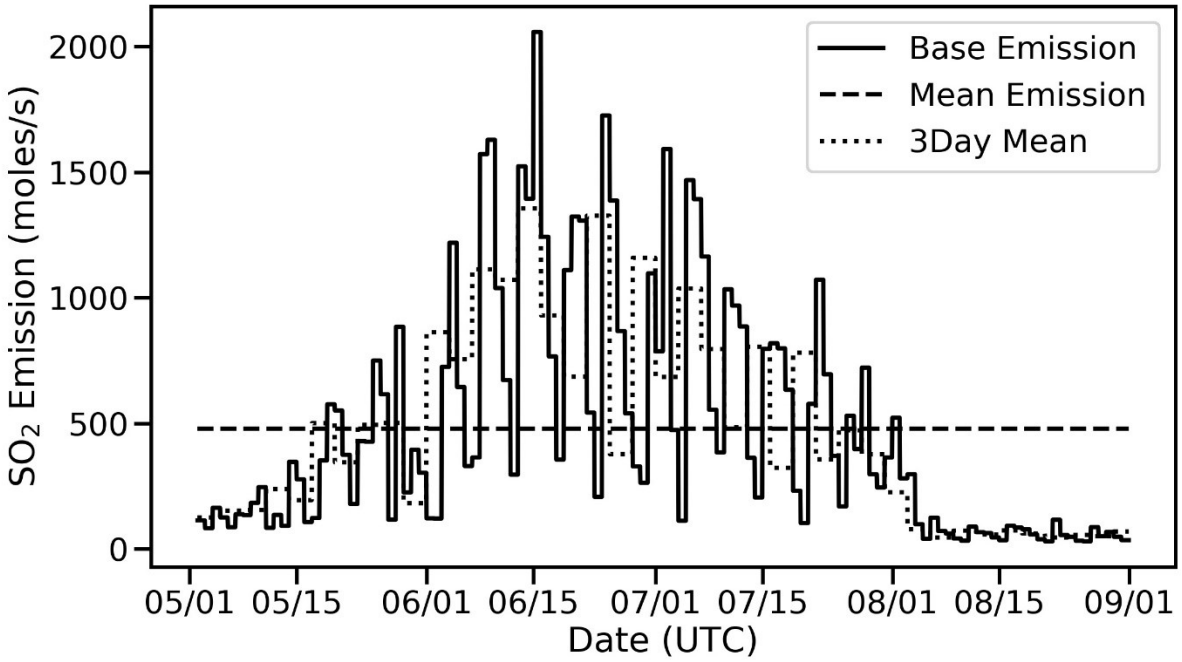

Figure 2. Estimated Hawaii regional SO_2 emission time series using OMPS SO_2 data (base emission), whole-period mean and the 3-day mean emissions.

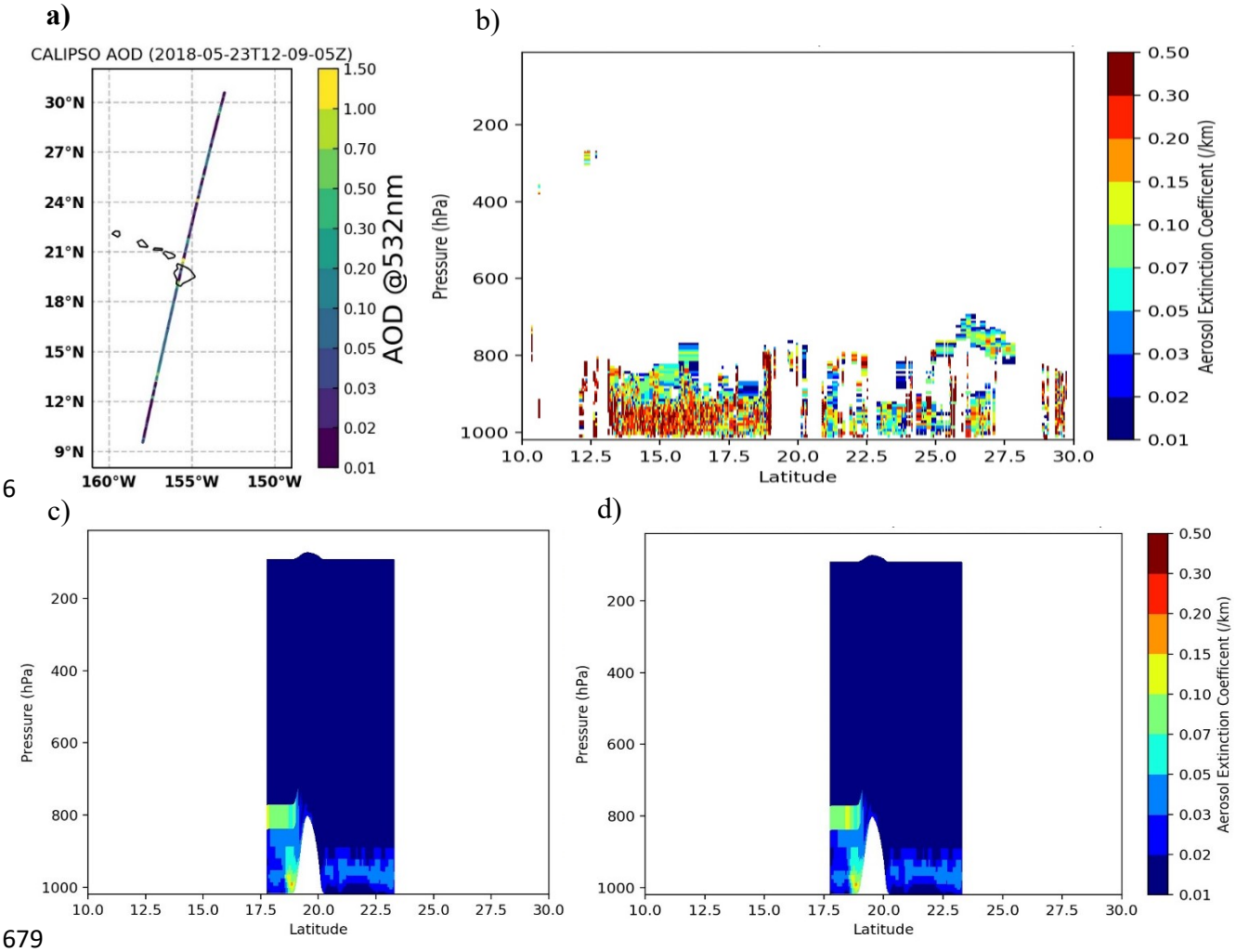

Figure 3, CALIOP path and retrieved aerosol optical depth (AOD) (a), and vertical profile of aerosol optical extinction coefficient (AOE) (b), and modeled AOE: Base (c) and "No Plume Rise" (d) runs, on 05/23/2018.

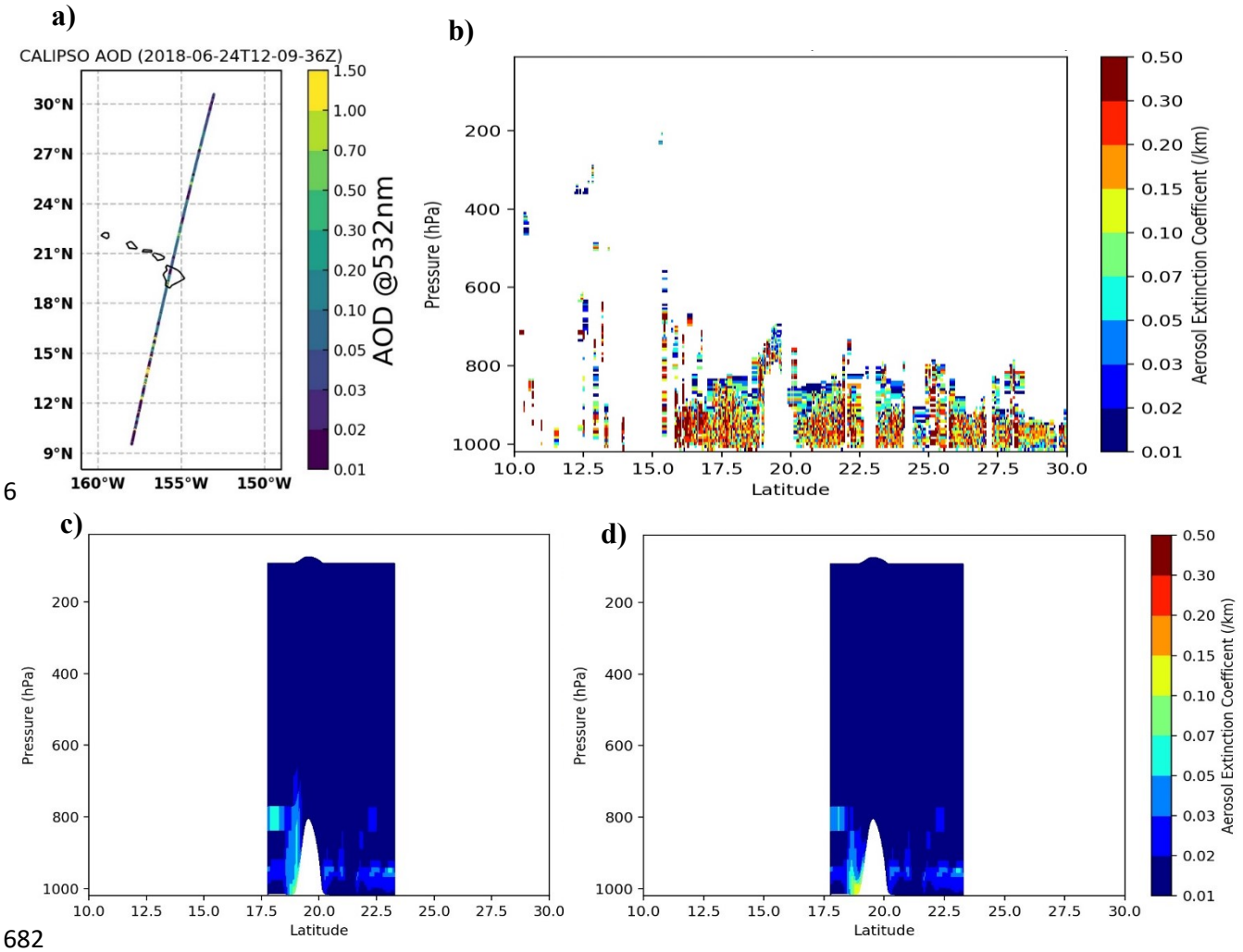

Figure 4, same as figure 3 but for 06/24/2018

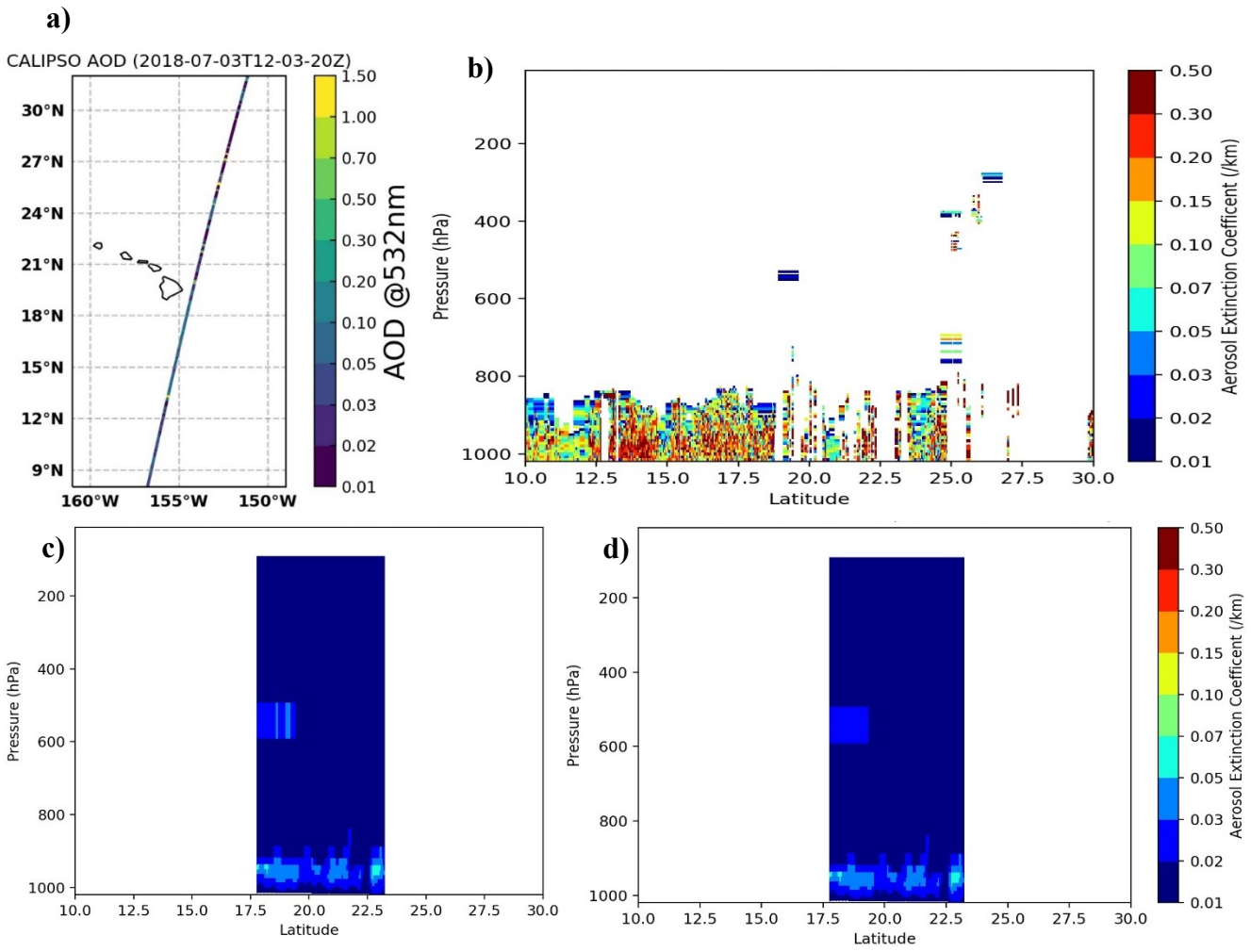

Figure 5, same as figure 3 but for 07/03/2018

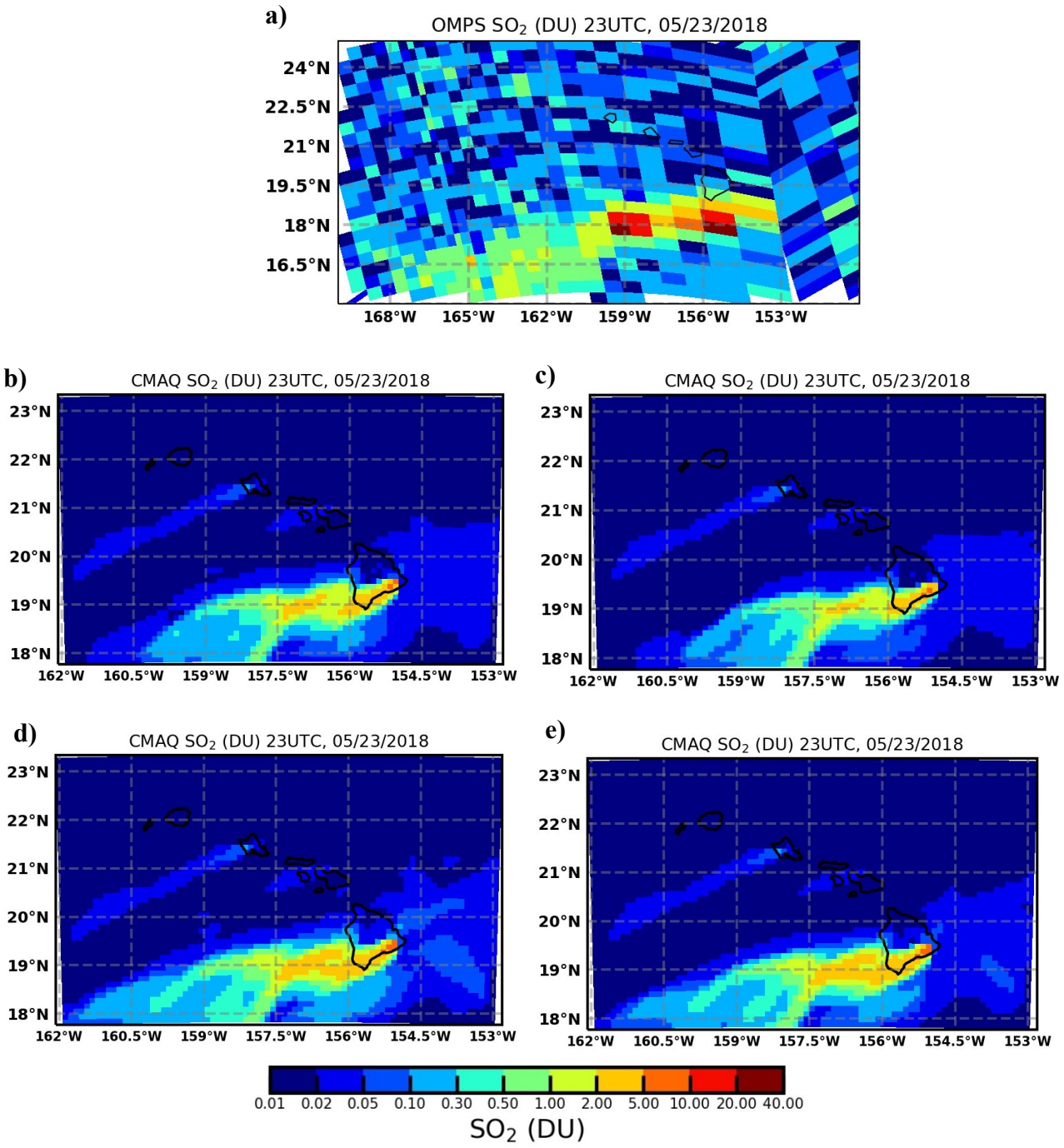

Figure 6. OMPS SO_2 (Dobson unit) (a) compared with the CMAQ simulations: b) Base run, c) No Plume Rise Run, d) Whole Period Mean, and e) 3-day mean, on 05/23/2018.

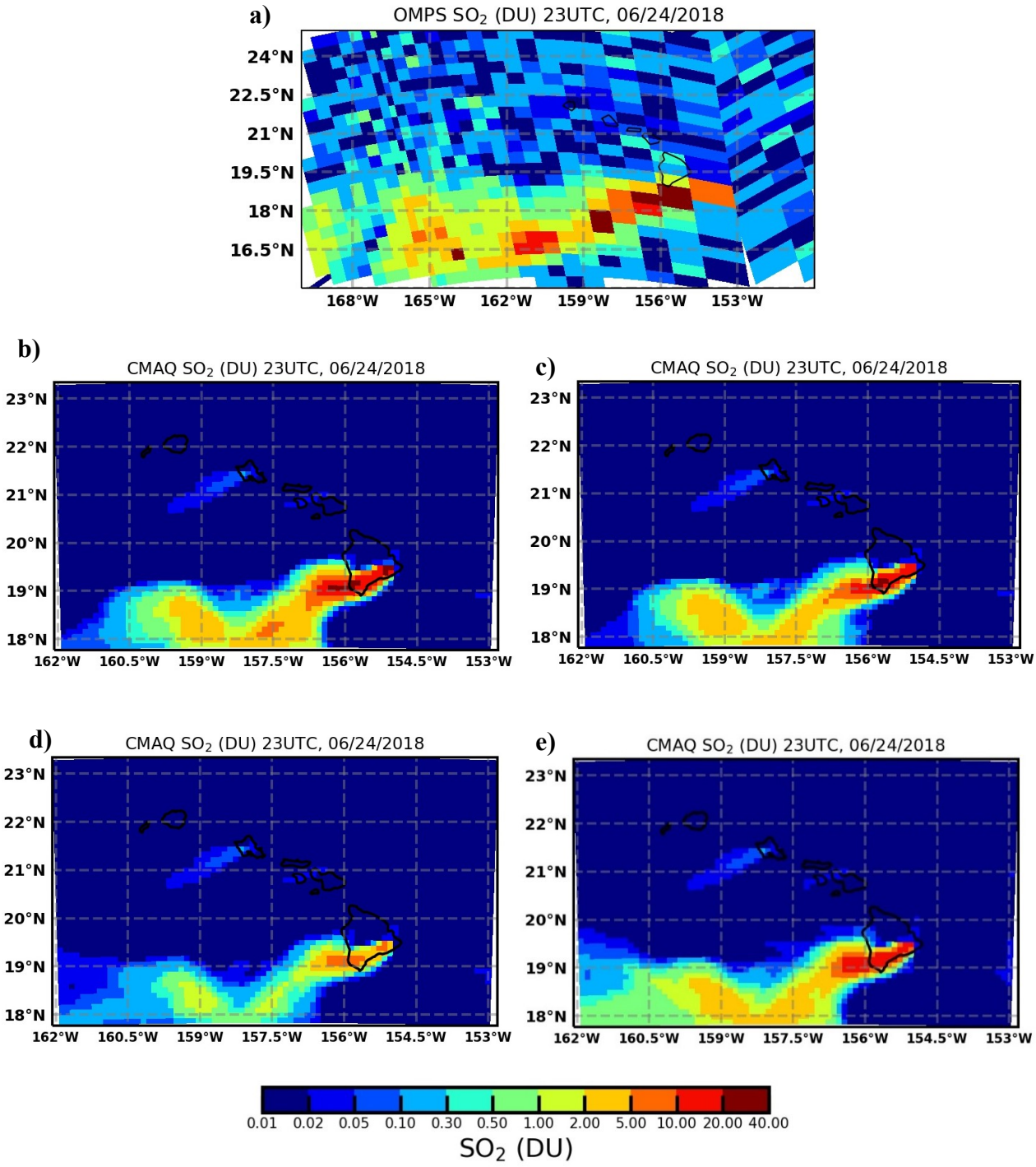

Figure 7. Same as Figure 6 but for 06/24/2018

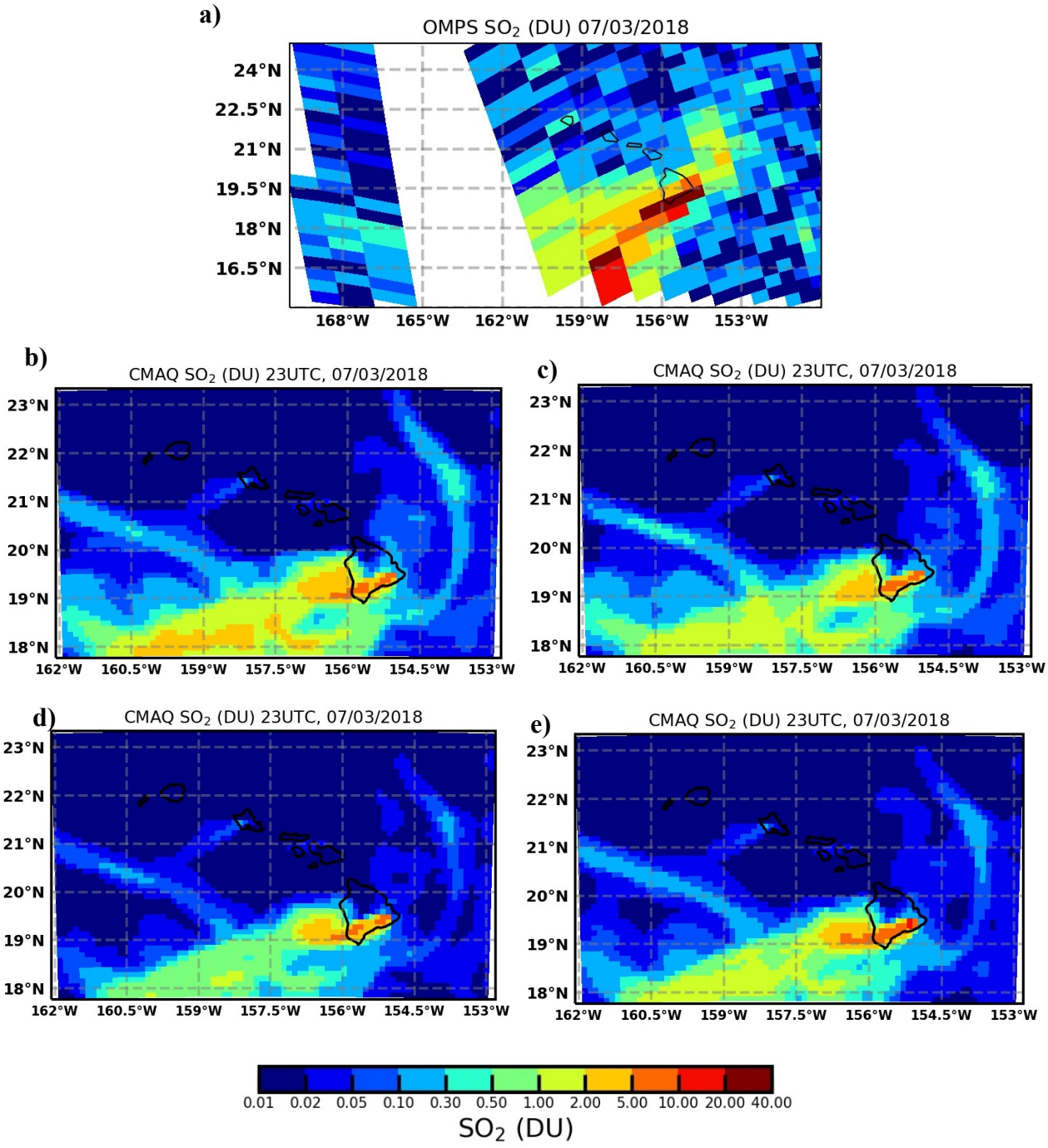

Figure 8. same as Figure 6 but for 07/03/2018.

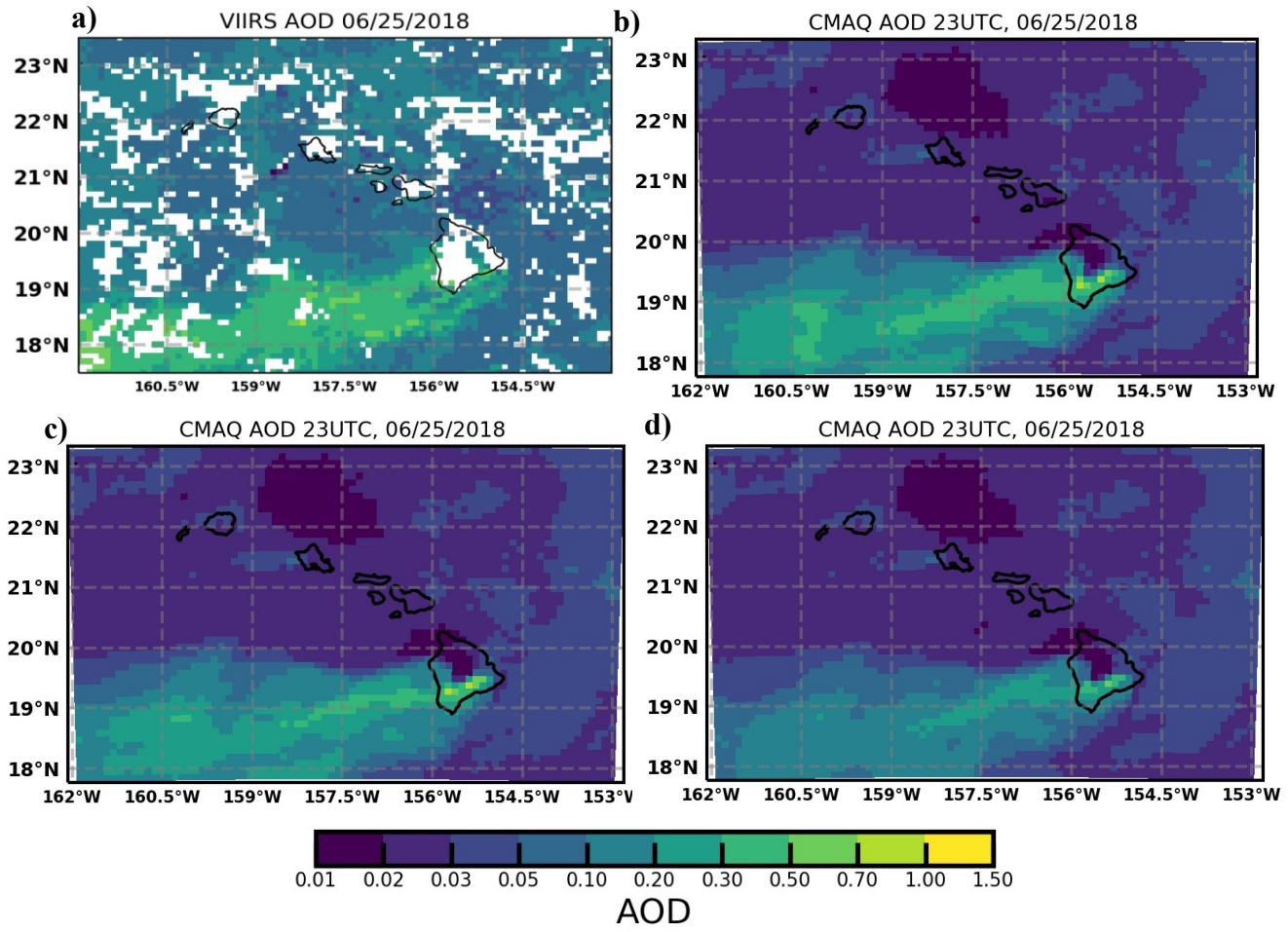

Figure 9. VIIRS AOD (a) compared with the CMAQ simulations: b) Base run, c) No Plume Rise run, and d) Whole-Period Mean Emission, on 06/25/2018

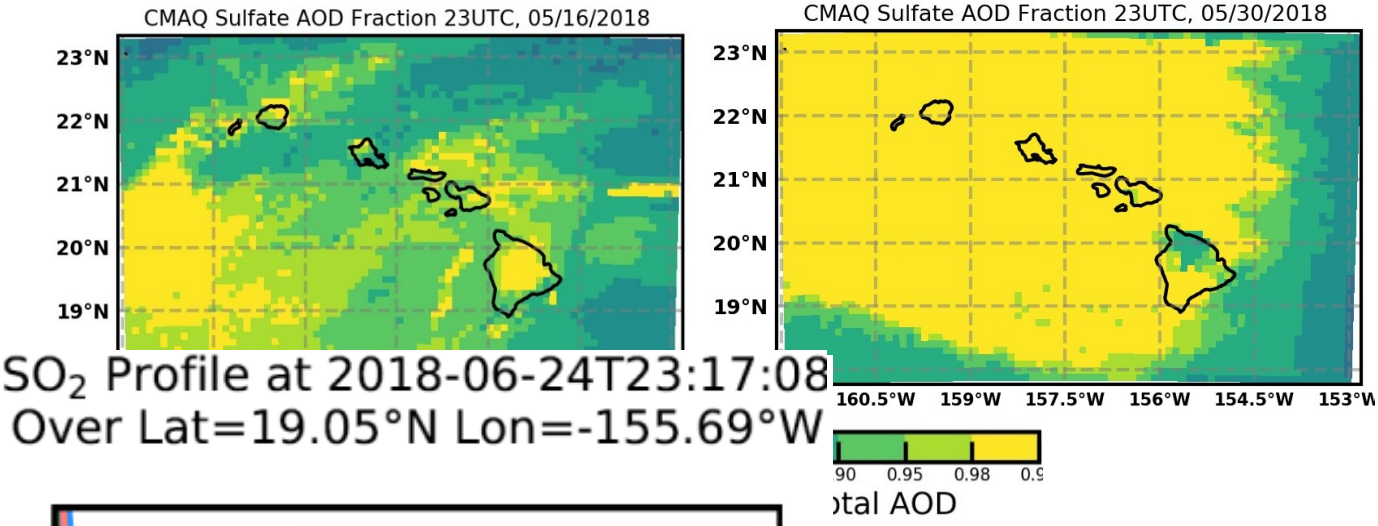

l AOD from the Base run on 05/16 and

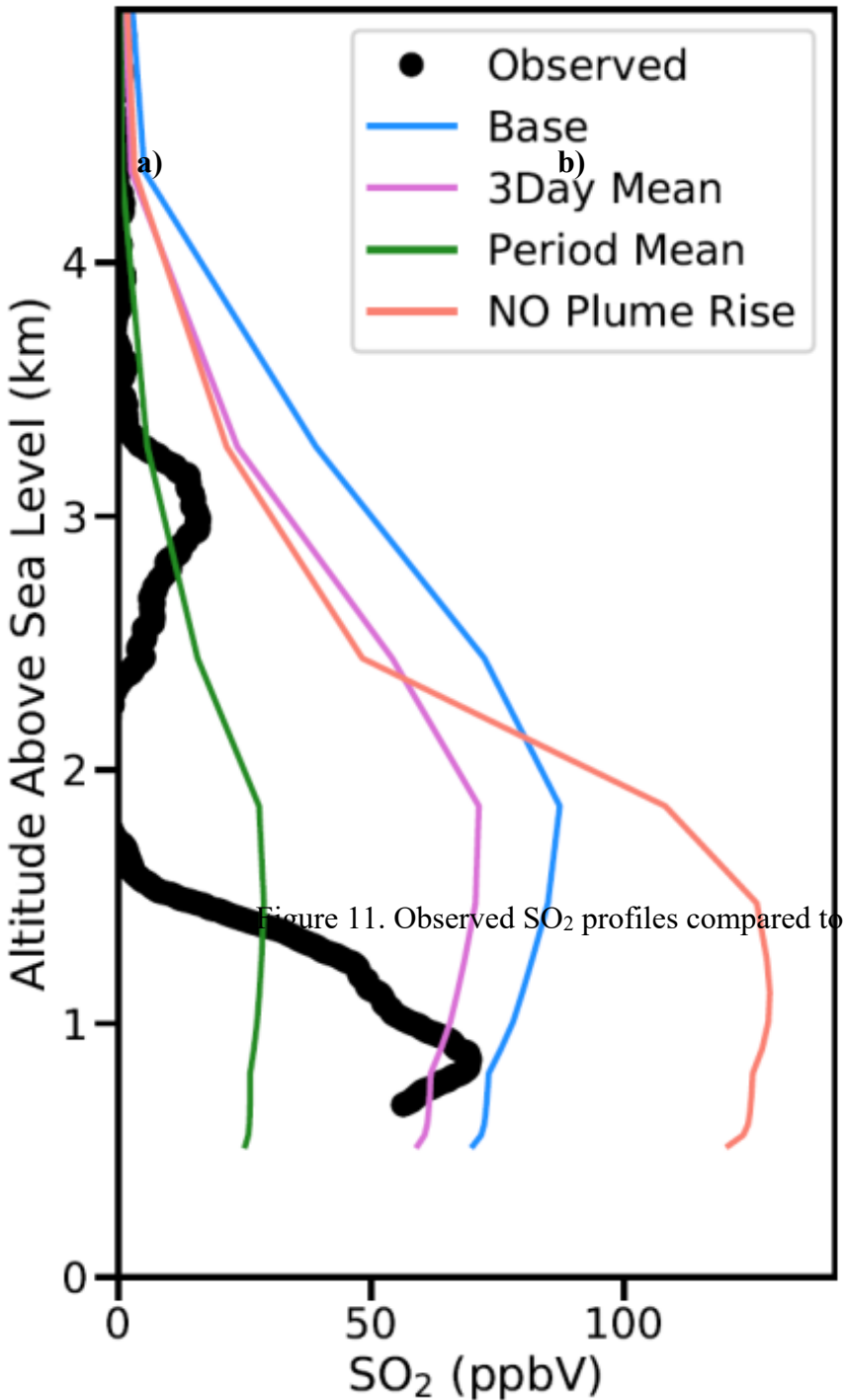

Figure 11. Observed SO_2 profiles compared to the 4 CMAQ runs for 3 scenarios.

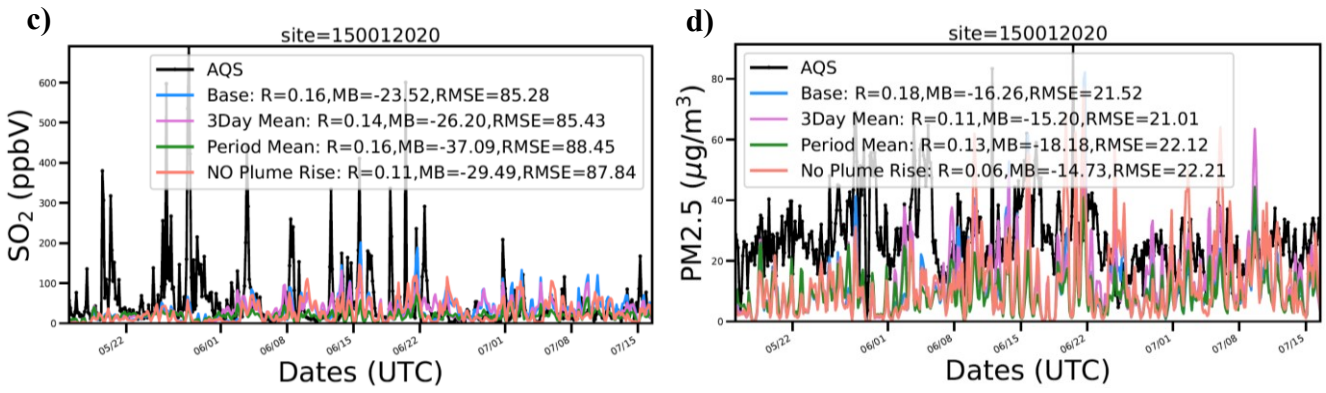

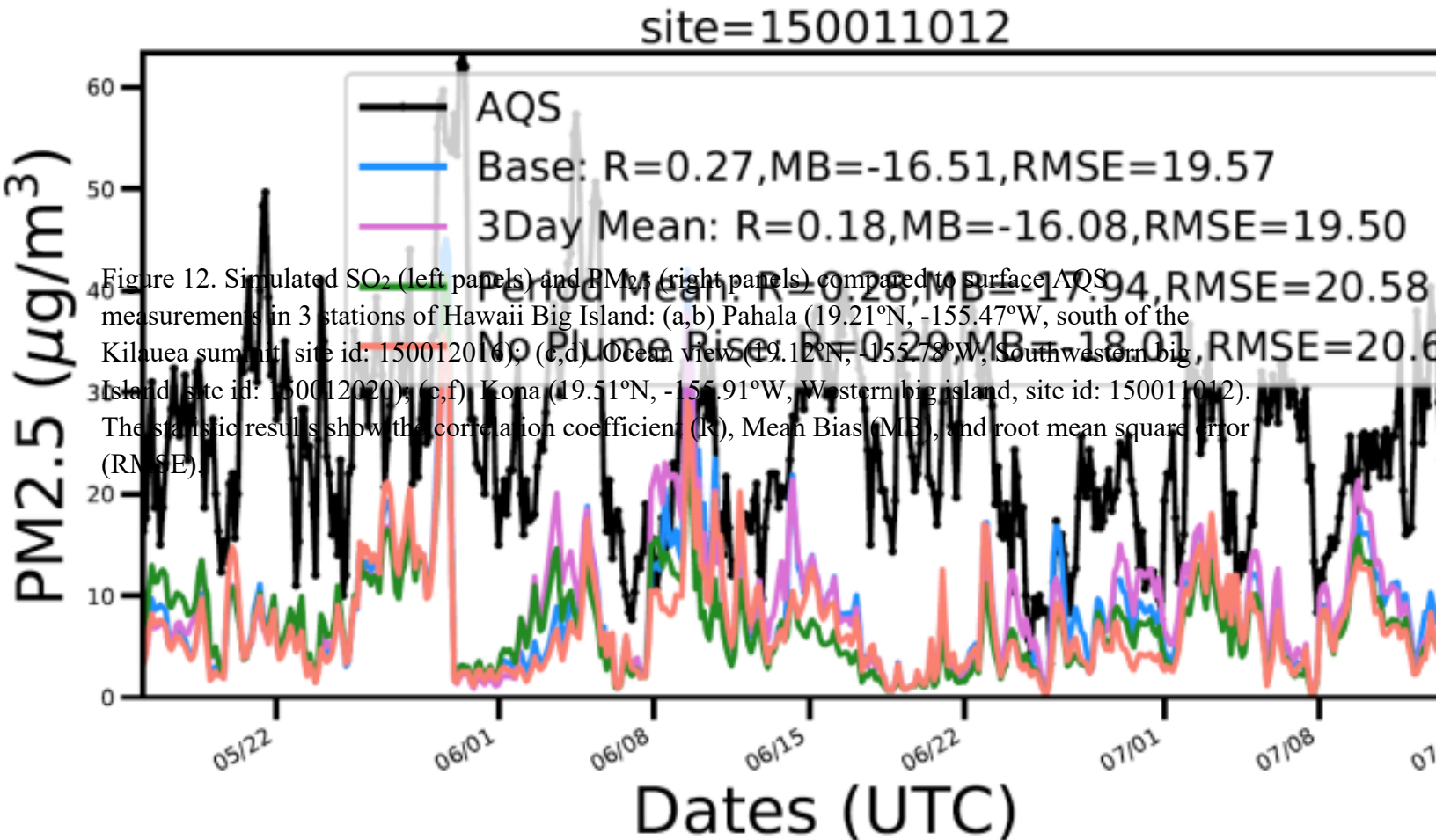

Figure 12. Simulated SO_2 (left panels) and $PM_{2.5}$ (right panels) compared to surface AQS measurements in 3 stations of Hawaii Big Island: (a,b) Pahala (19.21ºN, -155.47ºW, south of the Kilauea summit, site id: 150012016); (c,d) Ocean view (19.12ºN, -155.78ºW, Southwestern big Island, site id: 150012020); (e,f) Kona (19.51ºN, -155.91ºW, Western big island, site id: 150011012). The statistic results show the correlation coefficient (R), Mean Bias (MB), and root mean square error (RMSE).

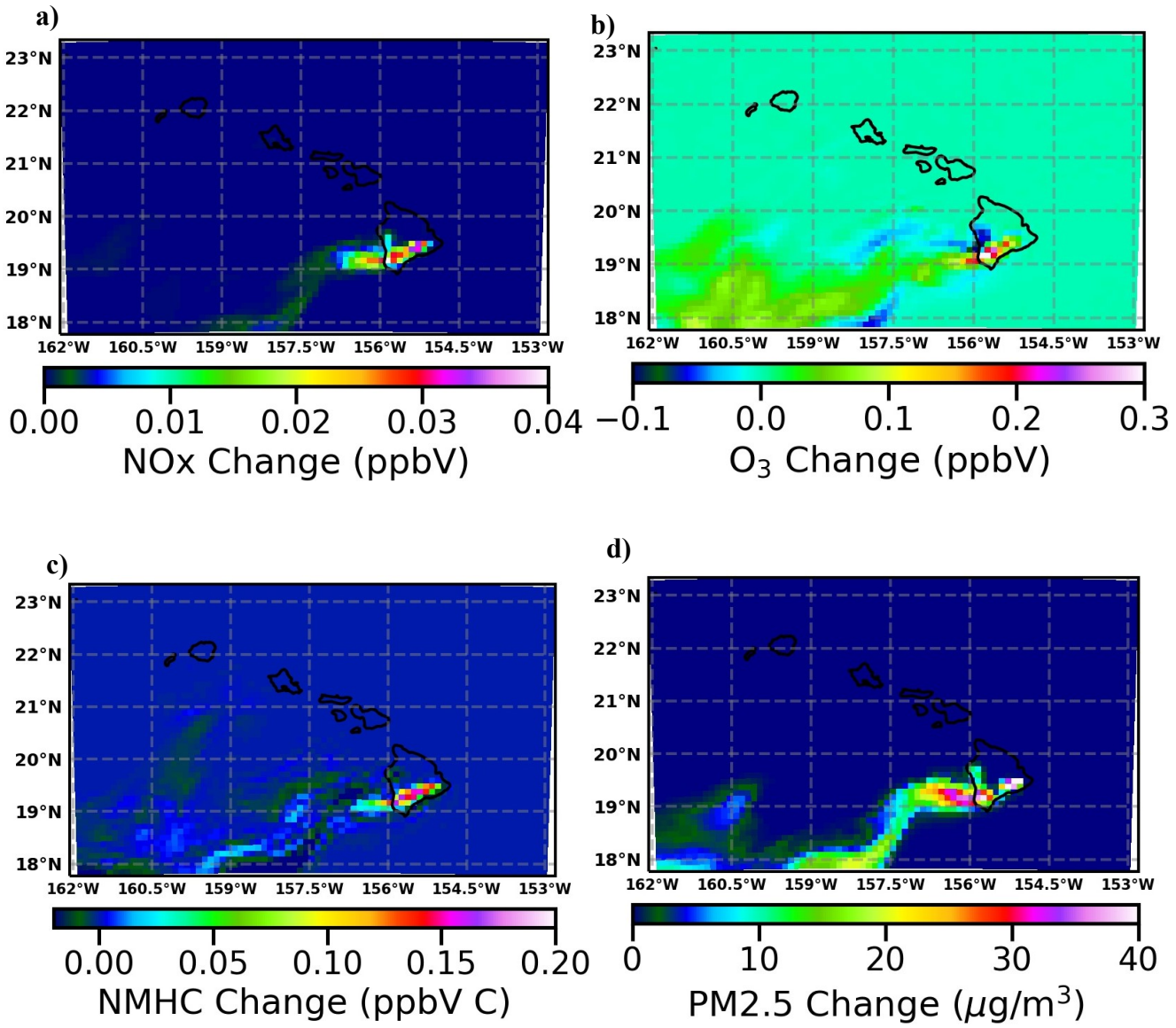

Figure 13, Surface concentration changes due to the volcano eruption at 23UTC, 06/25/2018 for NOx (a), O_3 (b), total non-methane hydrocarbons (NMHC) (c) and PM2.5 (d).

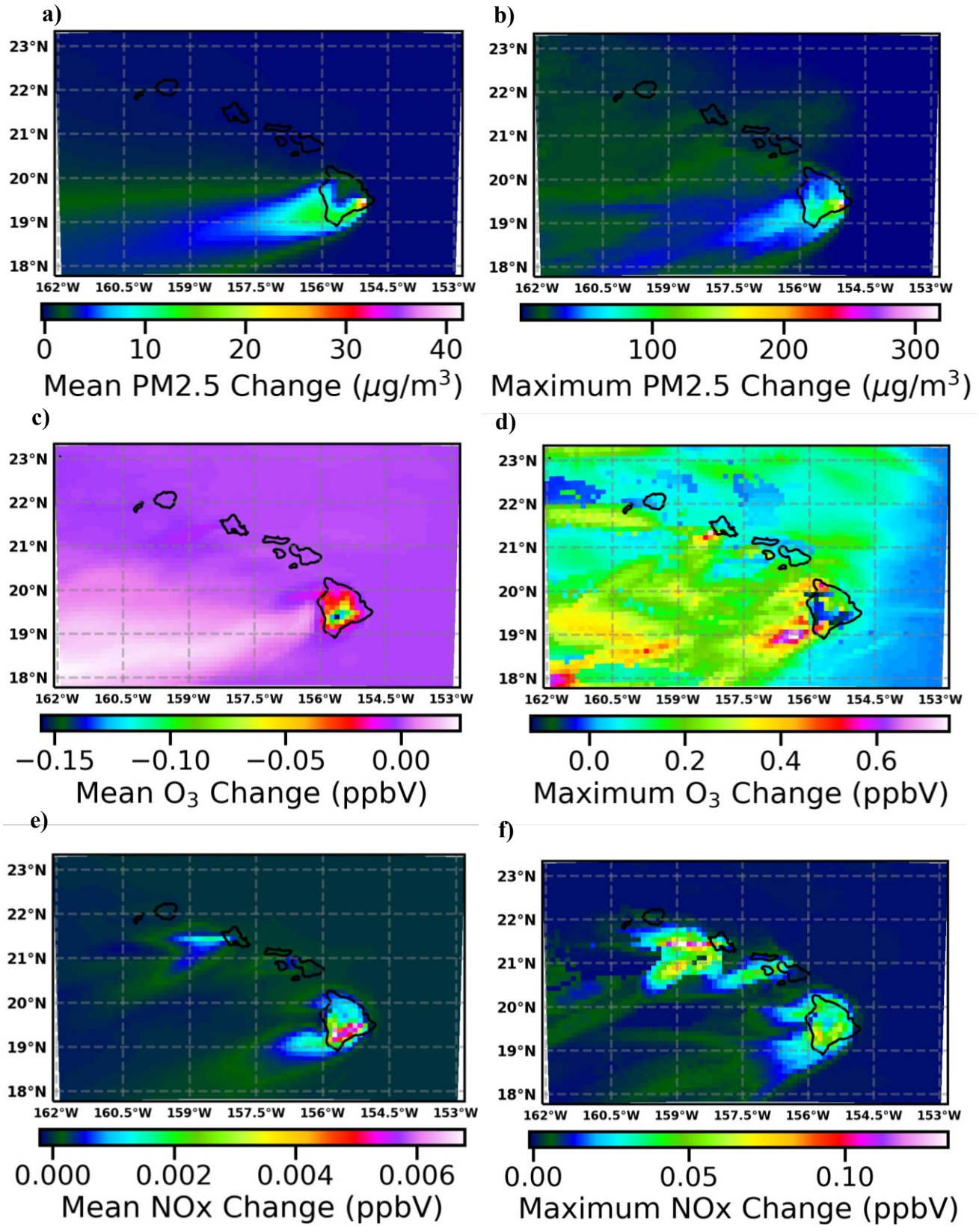
a)
b)
c)
d)
e)
f)
23°N
22°N
21°N
20°N
19°N
18°N
162°W 160.5°W 159°W 157.5°W 156°W 154.5°W 153°W
0 10 20 30 40
Mean PM2.5 Change (μg/m3)
100 200 300
Maximum PM2.5 Change (μg/m3)
−0.15 −0.10 −0.05 0.00
Mean O3 Change (ppbV)
0.0 0.2 0.4 0.6
Maximum O3 Change (ppbV)
0.000 0.002 0.004 0.006
Mean NOx Change (ppbV)
0.00 0.05 0.10
Maximum NOx Change (ppbV)

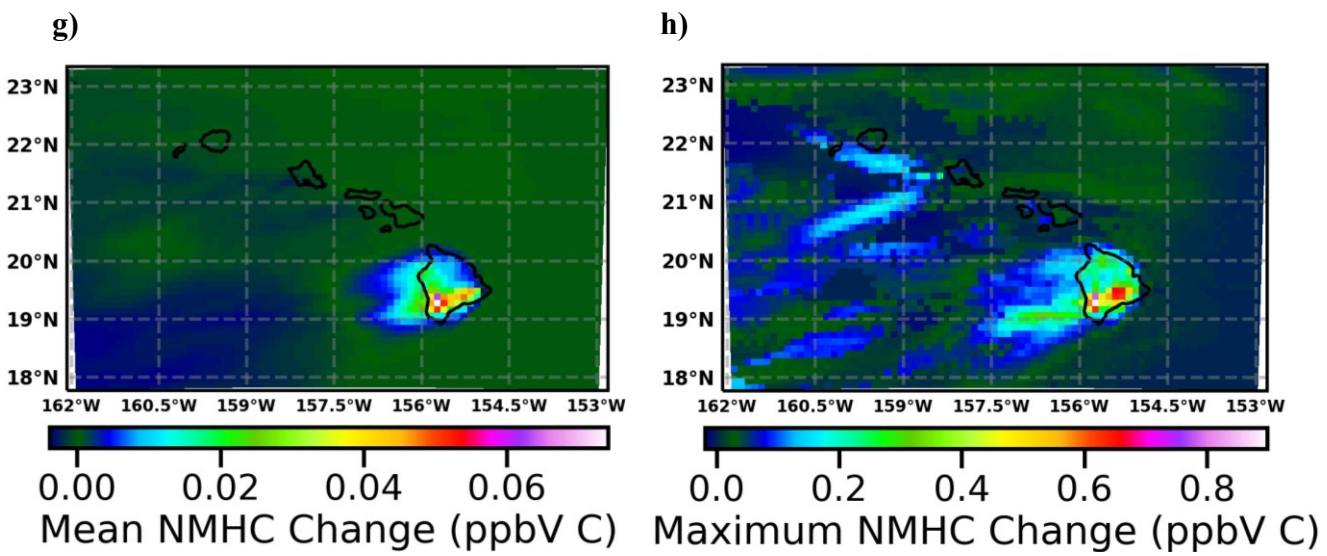

Figure 14, Impact of volcanic eruption on average (left) and maximum (right) surface concentrations of $PM_{2.5}$, O_3, NO_x and VOCs from May 12 to July 15, 2018 over Hawaii.